




## Article

# Prospect Evaluation of the Cretaceous Yageliemu Clastic Reservoir Based on Geophysical Log Data: A Case Study from the Yakela Gas Condensate Field, Tarim Basin, China

Wakeel Hussain <sup>1,2</sup>, Muhsan Ehsan <sup>3,\*</sup> , Lin Pan <sup>2,\*</sup>, Xiao Wang <sup>2</sup> , Muhammad Ali <sup>1</sup> , Shahab Ud Din <sup>4</sup>, Hadi Hussain <sup>2</sup>, Ali Jawad <sup>1</sup>, Shuyang Chen <sup>5</sup>, Honggang Liang <sup>5</sup> and Lixia Liang <sup>5</sup>

<sup>1</sup> School of Geophysics and Geomatics, China University of Geosciences, Wuhan 430074, China

<sup>2</sup> Department of Petroleum Engineering, Faculty of Earth Resources, China University of Geosciences, Wuhan 430074, China

<sup>3</sup> Department of Earth and Environmental Science, Bahria University, Islamabad 44000, Pakistan

<sup>4</sup> Faculty of Petroleum Engineering, China University of Petroleum, Beijing 102249, China

<sup>5</sup> SinoPEC Northwest Oilfield Company, Urumqi 830011, China

\* Correspondence: muhsanehsan98@hotmail.com (M.E.); panlin@cug.edu.cn (L.P.)

**Abstract:** This paper evaluated the oil and gas potential of the Cretaceous Yageliemu clastic reservoir within the Yakela condensed gas field lying in the Kuqa Depression, Tarim Basin, China. The petrophysical properties of the interest zones in the Kuqa area were characterized using geophysical logs from five wells. The results reveal that the gas-bearing zones are characterized by high resistivity, good permeability (K) and effective porosity ( $\Phi_{eff}$ ), low water saturation ( $S_w$ ), and low shale concentration ( $V_{sh}$ ), reflecting clean sand. The shale distribution model showed that these shales have no major influence on porosity and fluid saturation. The average shale volume, average effective porosity, and hydrocarbon saturation indicate that the Cretaceous Yageliemu Formation in the studied area contains prospective reservoir properties. The spatial distribution of petrophysical parameters, reservoir rock typing (RRT), and lithofacies were analyzed using the cross plots of litho saturation (volumetric analysis), iso-parametric representations of the petrophysical characteristics, cluster analysis, and self-organizing feature maps, respectively. The southeastern and northeastern regions of the research area should be ignored because of their high water and shale concentrations. The sediments in the southwest and northwest include the most potential reservoir intervals that should be considered for the future exploration and development of oil and gas fields in the study area.

**Keywords:** petrophysical analysis; well logs; Cretaceous reservoir; Yakela gas condensate field



**Citation:** Hussain, W.; Ehsan, M.; Pan, L.; Wang, X.; Ali, M.; Din, S.U.; Hussain, H.; Jawad, A.; Chen, S.; Liang, H.; et al. Prospect Evaluation of the Cretaceous Yageliemu Clastic Reservoir Based on Geophysical Log Data: A Case Study from the Yakela Gas Condensate Field, Tarim Basin, China. *Energies* **2023**, *16*, 2721. <https://doi.org/10.3390/en16062721>

Academic Editors: Xia Yan, Qi Zhang and Lijun Liu

Received: 24 January 2023

Revised: 8 March 2023

Accepted: 13 March 2023

Published: 14 March 2023



**Copyright:** © 2023 by the authors. Licensee MDPI, Basel, Switzerland. This article is an open access article distributed under the terms and conditions of the Creative Commons Attribution (CC BY) license (<https://creativecommons.org/licenses/by/4.0/>).

## 1. Introduction

The study of petroleum and reservoir systems in geological formations from the unidimensional perspective is called petrophysics [1–5]. In reservoir evaluation, petrophysical analysis plays an important role in discriminating between productive and nonproductive zones [6–11]. The use of geophysical logs and petrophysical analysis can distinguish various lithological groups that can be employed as a central concept for further exploration [12,13]. In order to process geophysical log data into physical parameters such as shale content, permeability, porosity, water, and hydrocarbon saturation, petrophysical interpretation is used. Effective evaluation of these reservoir parameters would help to delineate between hydrocarbon- and nonhydrocarbon-bearing zones [14,15].

Furthermore, formation evaluation is used to understand the wellbore geology at high resolution and assess the producible petroleum reservoir [16]. Due to the complexities of the reservoir environment and the subsequent diagenesis effectiveness, formation assessment is still a challenge in many fields [17–19]. Once the formation analysis is carried out on the reservoir, it is appropriate to take into account the location of the potential reservoir

interval in the drilled section, the estimation of the type of fluid existing in the void space, the saturation of each fluid, and the mobility of the fluids through the connected void space. To better achieve such comprehension, it is necessary to understand the petrophysical parameters because these properties are critical to understanding the essence of the reservoir and contribute to field development [15,20,21].

With a large number of proven oil and natural gas reserves, the Tarim Basin is a prominent petroleum provider in China that has contributed to the country's oil and gas sector for decades. The Yakela gas field, with an area of 390 km<sup>2</sup>, is a large high-pressure gas condensate field. It is geologically located north of the Tarim Basin, east of the Shaya Upwarping which is part of the Luntai Yakela Faulted Uplift zone [22,23]. There are no dynamic source strata in the Yakela Faulted Uplift; however, the bidirectional charging of oil and gas through the cratonic region and Kuqa Depression allowed for the accumulation of both marine and nonmarine hydrocarbons [24–28]. After the SC2 well discovery development in 1984, numerous moderate- to small-sized oil and natural gas reserves were explored [29–32]. Most of them are alongside the Yan'an, Lunati, and Yakela faults [33–35]. This encouraged us to further explore the present gas-prone intervals in this area. Recent research carried out in this area has shown that the rock structural complexities, heterolithic sequences, and burial depth of the Cretaceous Yageliemu Formation all affect one's potential to estimate reservoir properties by using well logs [36]. Furthermore, despite the many oil and gas discoveries in various parts along the Yakela Faulted Uplift zone, there is a lack of documentation on the detailed petrophysical studies there. Therefore, the present study's main focus is to evaluate the oil and gas prospects of the Lower Cretaceous Yageliemu clastic reservoir through detailed petrophysical analysis of wireline logs.

## 2. Geology of the Study Area

The Yakela gas condensate field lies in the Kuqa Depression, which is part of the northern Tarim Basin, in the northwest region of China (Figure 1a). The region is a faulted rock mass between the north of Yan'an and southern Luntai thrust faults (Figure 1b,c). The field is classified by three types of buried-hill hydrocarbon reservoirs [22,23], namely (i) a gas condensate reservoir in the Cretaceous Kabushaliang Formation, trapped in an anticline, (ii) a composite hydrocarbon condensate reservoir in a rock structure in the middle to lower Jurassic, and (iii) buried-hill-type oil condensate resources in the upper Proterozoic, upper Cambrian, and lower Ordovician, respectively. The nonclastic and clastic sedimentary rock types formed these geological structures (traps) for hydrocarbons. In contrast, the cap rocks consist of a predominantly mudstone lithology with shaly siltstone that was formed with evaporation salt in low sedimentation. The Jidike (N1j) Formation, Kapushaliang group, lower Jurassic, from Palaeozoic to Cenozoic, provides multiple seal rocks for reservoirs. Based on the geological settings and oil and gas reservoir properties, the Yakela gas condensate field is divided into four sectors [22,23]: (i) the oil and gas sector, (ii) the fault sector, which crosses the deep reservoirs in the Luntai fault, (iii) the oil and water sector, and (iv) an outer region, i.e., outside the northern gas field boundaries.

This study focuses on the Cretaceous Yageliemu Formation, which comprises upper and lower members. The lower segment is divided into lower 1 and lower 2 sub-segments from top to bottom. The stratigraphy of the Yageliemu Formation is parallel and unconformable to the Kalaza Formation of the Lower Jurassic and is in continuous contact with the overlying strata of the Shushanhe Formation. This area belongs to a typical alluvial fan-braided river delta sedimentary system. The lithology of the upper member is primarily feldspathic lithic fine sandstone, whereas the lower member consists of mainly gravelly coarse-grained arkose, fine-grained lithic arkose, sandy conglomerate, and fine sandstone [37,38]. Figure 2 shows the stratigraphic chart and petroleum system of the Tarim Basin.

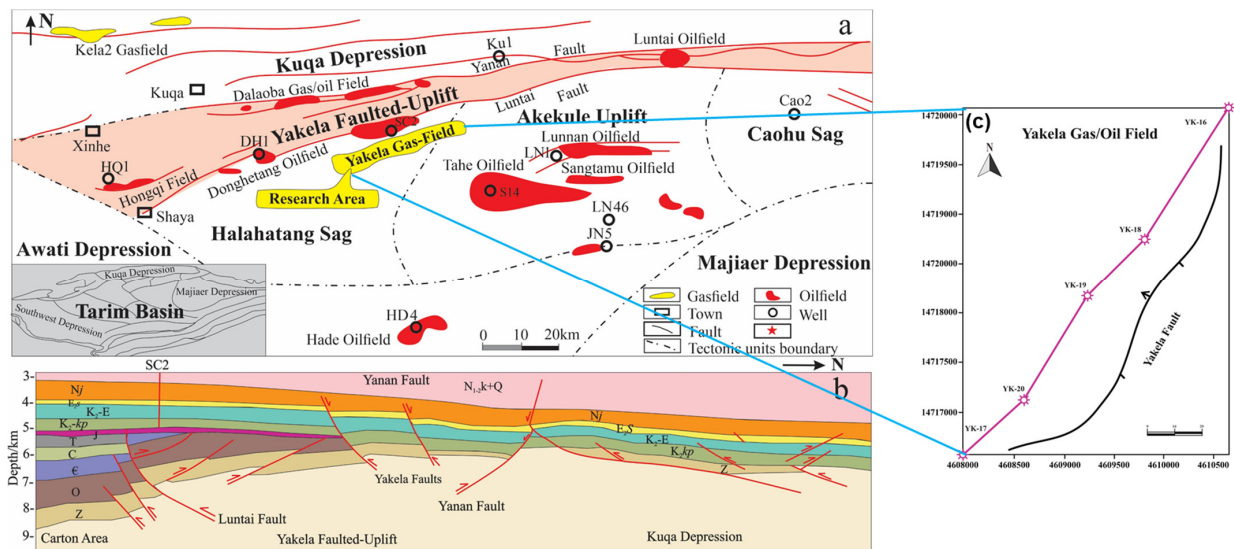


**Figure 1.** (a) Location of the Yakela gas field (research area), Faulted Uplift, and tectonic units of the Tarim Basin (b) Yakela Faulted Uplift schematic structural cross section and (c) the base map of interpreted wells, modified according to [23].

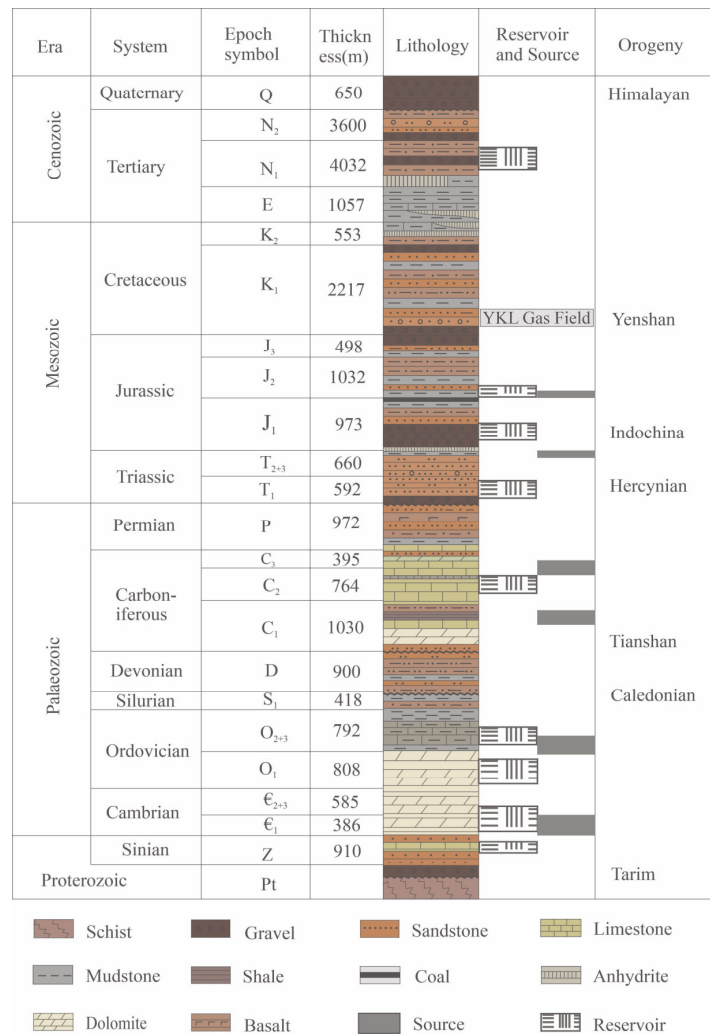


**Figure 2.** Generalized stratigraphic column of the Kuqa depression.

### 3. Materials and Methods

The present study is focused on a petrophysical evaluation utilizing well-log data of the Yageliemu clastic reservoir from five selected wells, namely YK16, YK17, YK18, YK19, and YK20. The composite geophysical logs, neutron-compensated log (CNL), density log (RHOB), Ac log, caliper log (CAL), self-potential log (SP), gamma ray log (GR), bit size (BS) deep resistivity (RILD), medium resistivity (RILM), and shallow resistivity (RFOC) were utilized to evaluate and characterize the zones of interest. The logs readings and litho saturation cross plots for well YK16 and YK18 in the Yageliemu Formation are illustrated in Figures 3 and 4. For petrophysical interpretation, geophysical log data files were imported to the IP<sup>®</sup> Interactive Petrophysics software and Surfer 2021. In the analysis of well logs, zoning is a fundamental step. The logs were split into productive and nonproductive zones of the reservoir. The zones of the interest evaluation process were constructed from the geophysical log analysis, based on cross plots, isoperimetric maps, pre-established calculations/formulas, and charts. Figure 5 indicates the methodological workflow for the present study, which is described below:

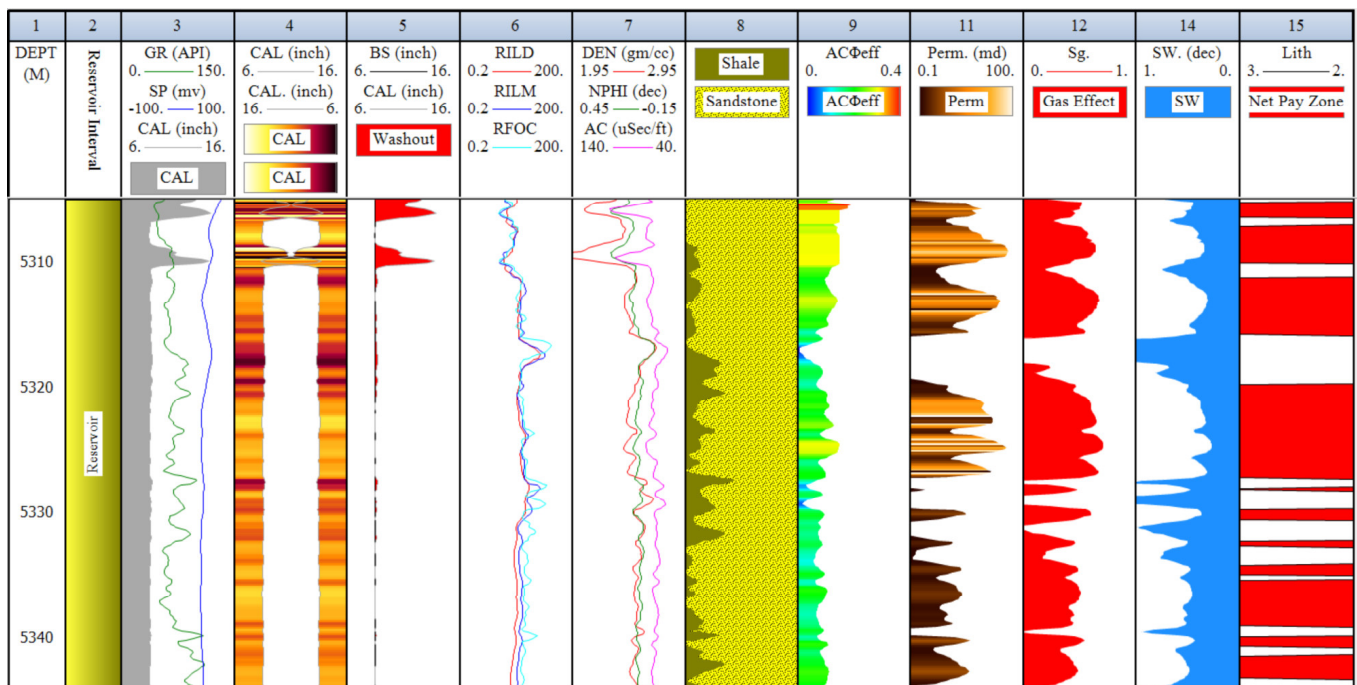


**Figure 3.** The conventional log overview and litho saturation cross plot of YK16 in the Yakela gas condensate field indicates that the current research Formation (zones) reveals a significant number of sub-reservoir gas zones, where the average water saturation value is 36 percent.



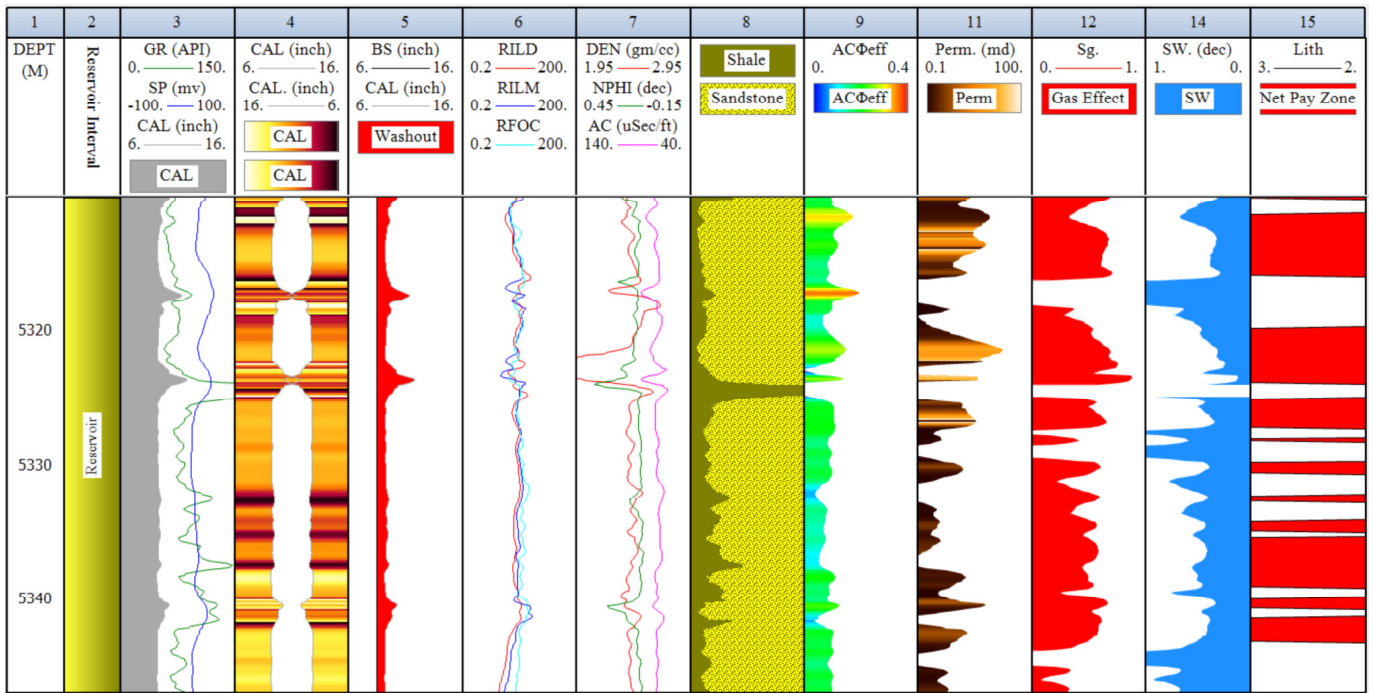


Figure 4. Litho saturation cross plot for YK18.

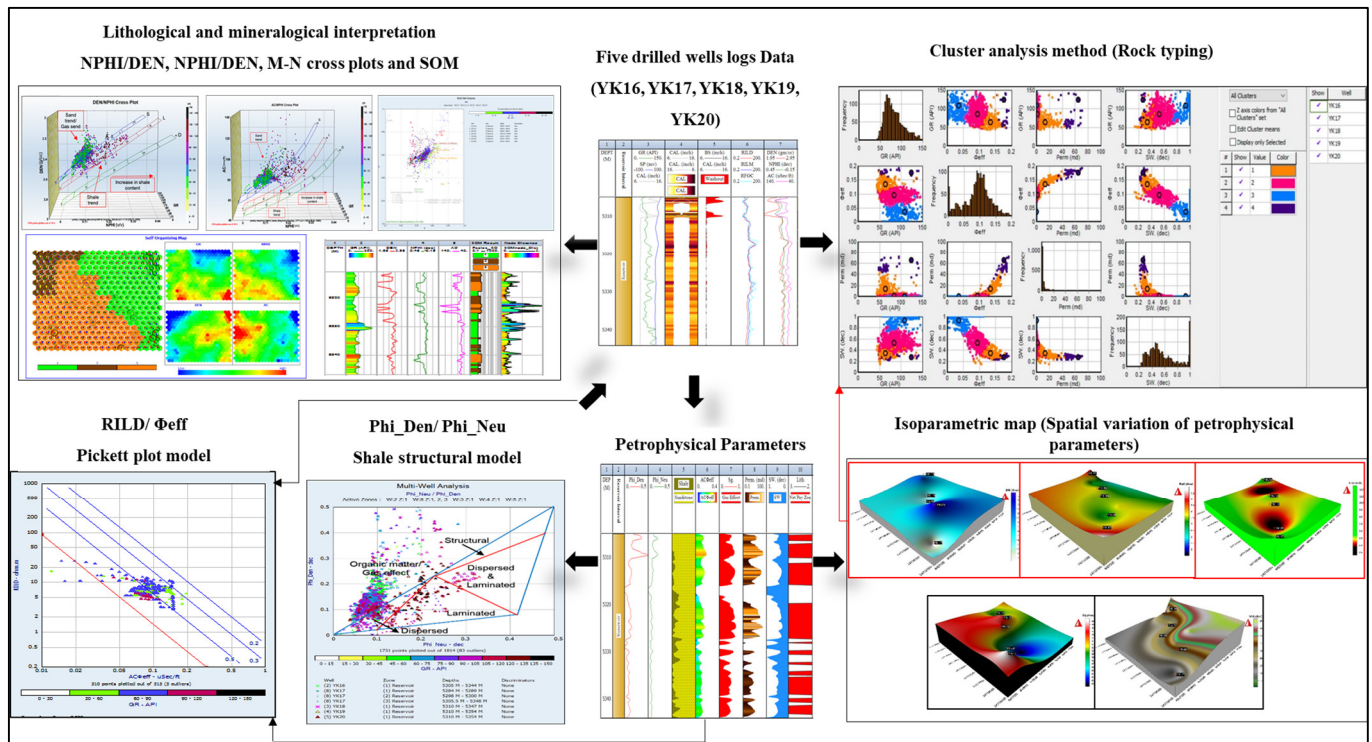


Figure 5. Workflow for analyzing and characterizing the study reservoir.

### 3.1. Petrophysical Parameters

#### 3.1.1. Shale Volume

The first significant step in the petrophysical assessment was to compute the shale volume as a function of depth. The Yageliemu Formation is lacking radioactive materials,

hence gamma-ray logs could be used to determine the shale volume fraction [39]. The IGR (gamma ray index) can be described as an equation (Equation (1)).

$$\text{IGR} = \frac{\text{GR}_{\text{Log}} - \text{GR}_{\text{min}}}{\text{GR}_{\text{max}} - \text{GR}_{\text{min}}} \quad (1)$$

where  $\text{GR}_{\text{max}}$  means maximum gamma ray log value (100% shale),  $\text{GR}_{\text{min}}$  means minimum gamma ray log value (shale-free sandstone), and  $\text{GR}_{\text{Log}}$  shows gamma-ray log response in the identified sand packages. The gamma-ray logs are usually recorded in API units (American Petroleum Institute).

Some geophysicists assume that the shale index is equivalent to the shale content. However, it tends to overestimate the shale volume. In order to provide more reliable shale volume estimates, a precise relationship was thus constructed for different geologic areas and eras. Clavier et al. [40] developed a relationship for computing the shale volume accurately in the formation. This method provides a more accurate volume of shale to minimize the misinterpretation due to the occurrence of hot sands [41] (Sands with a certain radioactive material content, normally potassium or thorium, which indicates high gamma ray log values) (Equation (2)).

$$V_{\text{sh}} = [1.7 - (\text{IGR} + 0.7)^2]^{1/2} \quad (2)$$

### 3.1.2. Porosities

Data for the density log and neutron log were unreliable due to borehole anomalies (washout/breakout). The caliper log revealed that the data quality was unsatisfactory. Therefore, we used the sonic log to calculate porosity. The porosity of the selected zones was calculated using the sonic Raymer porosity model (Equation (3)) and applied to each zone in each well [42].

$$\varnothing_{\text{S}} = \frac{\Delta t_{\text{log}} - \Delta t_{\text{ma}}}{\Delta t_{\text{fl}} - \Delta t_{\text{ma}}} \quad (3)$$

$$\varnothing_{\text{sh}} = \frac{\Delta t_{\text{sh}} - \Delta t_{\text{ma}}}{\Delta t_{\text{fl}} - \Delta t_{\text{ma}}} \quad (4)$$

Once the porosities were obtained using Equations (3) and (4), we estimated effective porosity from Equation (5).

$$\varnothing_{\text{eff\_Sonic}} = \varnothing_{\text{Sonic}} - V_{\text{sh}} * \varnothing_{\text{sh}} \quad (5)$$

where  $\varnothing_{\text{S}}$  = sonic derived porosity,  $\varnothing_{\text{sh}}$  = shale porosity,  $\Delta t_{\text{log}}$  = log reading,  $\Delta t_{\text{ma}}$  = matrix travel time, and  $\Delta t_{\text{fl}}$  = fluid travel time (freshwater mud = 189 us/ft; saltwater mud = 185 us/ft).

### 3.1.3. Permeability

The equation from the Morris–Biggs gas method was used to compute the permeabilities of the reservoir intervals [43] (Equation (6)).

$$K_{\text{MBG}} = 6241 * \frac{\varnothing e^6}{S_{\text{Wi}}^2} \quad (6)$$

where  $K_{\text{MBG}}$  = Morris–Biggs gas absolute permeability,  $\varnothing e$  = Effective porosity, and  $S_{\text{Wi}}$  = Irreducible water saturation.

### 3.1.4. Water Saturation

The most challenging and important petrophysical parameter is water saturation, from which the initial hydrocarbon concentration in the reservoir can be assessed throughout the formation evaluation [44–46]. To determine water saturation ( $S_{\text{w}}$ ), there are several techniques available. The methods most frequently used throughout the petroleum industry

are to calculate the ( $S_w$ ) of the field findings [47,48]. As the Cretaceous Yageliemu Formation is not shaly, the Archie equation is therefore best suited for estimating water saturation. The Pickett plot was used to analyze Archie's parameters as it is a visual depiction of Archie's equation and is consequently an excellent graphic tool to calculate  $S_w$  ranges inside a reservoir [49–51] (Equation (7)).

$$S_w = \left( \frac{a * R_w}{R_t * \phi_{eff}^m} \right)^{\frac{1}{n}} \quad (7)$$

where  $m$  = cementation exponent,  $n$  = saturation exponent, and  $a$  = tortuosity factor, while  $R_t$ ,  $R_w$ ,  $S_w$ , and  $\phi_{eff}$  indicate true formation resistivity, water resistivity, water saturation, and formation effective porosity, respectively.

### 3.1.5. Water Resistivity ( $R_w$ )

In the present work, the water resistivity ( $R_w$ ) was evaluated using the spontaneous potential (SP) log. As with many scenarios, a good estimate of formation water resistivity ( $R_w$ ) could be easily noticed by reading the SP curve in clean (non-shale) formations. The formula is as follows:

$$SSP = -K \log^* \frac{R_{mfe}}{R_{we}} \quad (8)$$

where  $SSP$  = static SP ( $SSP$ ) measurement,  $K$  = constant,  $R_{we}$  = equivalent formation water resistivity, and  $R_{mfe}$  = equivalent mud filtrate resistivity.

The calculated static SP value could be converted into the resistivity ratio  $R_{mfe}/R_{we}$  once the formation temperature was specified. When the resistivity ( $R_{mf}$ ) of a mud filtrate sample was obtained, the equivalent formation water resistivity ( $R_{we}$ ) could be calculated easily.

### 3.1.6. Gas Saturation

The gas saturation can be estimated by using the following equation [52] (Equation (9)).

$$S_g = 1 - S_w \quad (9)$$

where  $S_g$  = gas saturation and  $S_w$  = water saturation.

## 3.2. Cross-Plot-Based Lithological and Mineralogical Analysis

An essential aspect of reservoir assessment is the prediction of the matrix components. The lithological and mineralogical components of the Cretaceous Yageliemu Formation were interpreted using the neutron (NPHI)-density (RHOB), sonic (AC)-neutron (NPHI), neutron (NPHI)-gamma-ray (GR), and M-N cross plots. We used Equations (10) and (11) to calculate M-N, and the inputs required to predict M-N curves are given in Table 1.

$$M = \frac{(\Delta t_f - \Delta t_{ma})}{(\rho_{ma} - \rho_f)} * (0.01) \quad (10)$$

$$N = \frac{(\phi_{nf} - \phi_{nma})}{(\rho_{ma} - \rho_f)} \quad (11)$$

where  $M$  is the slope on the sonic and density cross plot of each lithology line,  $N$  is the slope on the neutron and density cross plot of the distinct lithology lines,  $\rho_{ma}$  = matrix density, and  $\rho_f$  = fluid density.

**Table 1.** Parameters used for MN calculation.

( $\mu\text{sec}/\text{ft}$ )	( $v/v$ )	( $\text{g}/\text{cc}$ )
$\Delta t_f$	$\Phi_{nf}$	$P_f$
189	1.0	1.0

### 3.3. Facies Evaluation

Electrofacies assessment is a significant step for accurate reservoir rock evaluation [53]. We used a type of artificial neural network (ANN) known as a self-organizing map (SOM) to minimize the uncertainties and analyze the electrofacies. The self-organizing map is an unsupervised learning model introduced by Kohonen [54]. The self-organizing map (SOM) can be described by Equation (12).

$$W_v(s+1) = W_v(s) + \theta(u, v, s) \cdot \alpha(s) \cdot [D(t) - W_v(s)] \quad (12)$$

where  $s$  = current iteration,  $t$  = index of the target input data vector in the input dataset,  $D(t)$  = vector of the target input data,  $v$  = node index in the map,  $W_v(s)$  = current weight vector of node  $v$ ,  $u$  = best matching units (BMUs) index on the map (node in the SOM with the minimum aggregate distance to an input vector),  $\theta(u, v, s)$  = restraint owing to the distance from BMUs, typically called the neighborhood, and  $\alpha$  = learning restraint on account of iteration progress.

### 3.4. Reservoir Rock Typing

Reservoir rock typing quality evaluation is an essential factor in the oil industry because it regulates reservoir output [55,56]. This study used a cluster analysis approach to determine the reservoir rock typing quality.

There are various processes in this method that clusters should join at each point. The key approaches are summarized as follows.

#### 3.4.1. Nearest Neighbor Approach

This case shows the cluster “closest” to another cluster (minimum distance between two data points).

#### 3.4.2. Furthest Neighbor Approach

This method indicates the data point “furthest” from another data point (maximum distance between two neighbors).

#### 3.4.3. Average Approach

The distance is computed as the mean distance between the two clusters for all subjects' pairs. The space between the two objects may be calculated using the Euclidean approach as follows [57] (13).

$$xy = \sqrt{\sum_{i=1}^n (x_i - y_i)^2} \quad (13)$$

where  $x$  and  $y$  are two key positions in Euclidean  $n$  space, Euclidean vectors are  $x_i$  and  $y_i$ , beginning from the origin, and  $n$  indicates  $n$  space.

## 4. Results and Discussion

### 4.1. Lithological and Mineralogical Evaluation

#### 4.1.1. Cross-Plot-Based Lithological Evaluation

In the absence of core sample data, the log response is an efficient tool for assessing the insight binary or ternary mixtures of lithologies and evaluating the reservoir rocks' productive and nonproductive zones [58]. In well log interpretation, cross plots are a useful approach to visualize how the various combinations of logs respond to different lithologies. Such cross plots and estimations based on them are extremely helpful, but these plots' interpretations sometimes becomes ambiguous when the lithology is complex.

In the present study, neutron-density, neutron-sonic, and neutron-gamma-ray log cross plots (Figures 6–8) were employed to identify the lithological components and predict the fluid type present at the zone of interest (reservoir level). To simplify the work of distinguishing lithofacies, an indication of clean sandstone (reservoir) zones and the potential increase in clay/shale volume was provided by the gamma-ray values on the  $z$ -axis. The

distribution of data points occurs from the well logs among the respective lithological lines (sandstone, limestone, and dolomite). Therefore, various pieces of log data can be combined to provide valuable clues and observations of subsurface lithologies. A cross plot of the acoustic, density, neutron, and gamma ray logs was plotted for each well. These cross plot results were also likened to the SOM method to examine lithology effectively.

The scattering of each data point from each well indicates the same pattern. The prominent points on both neutron-density and neutron-sonic cross plots (Figures 6 and 7) suggest sandstone with some shale and clay is the predominant reservoir lithology. Clay in sandstone leads data points toward the shale region that lies beneath the sandstone line.

In the neutron-gamma ray cross plot (Figure 8), the point distribution indicates the same lithology variation. Clean sandstone is characterized by the lowest gamma ray (approximately 60 API) and medium neutron log values, while shaly sandstone is indicated by moderate gamma ray (60 to 75 API) and neutron values. A gamma ray log response ranging from 75 to 90 API with neutron values lower than 0.25 is suggested for shaly sand. Intermediate gamma ray values but a greater neutron log response, i.e., higher than 0.20, shows the existence of lime, and very high gamma ray values (greater than 90 API) describe shale-rich contents. This characterization was carried out based on the analysis carried out by various researchers [59–62].

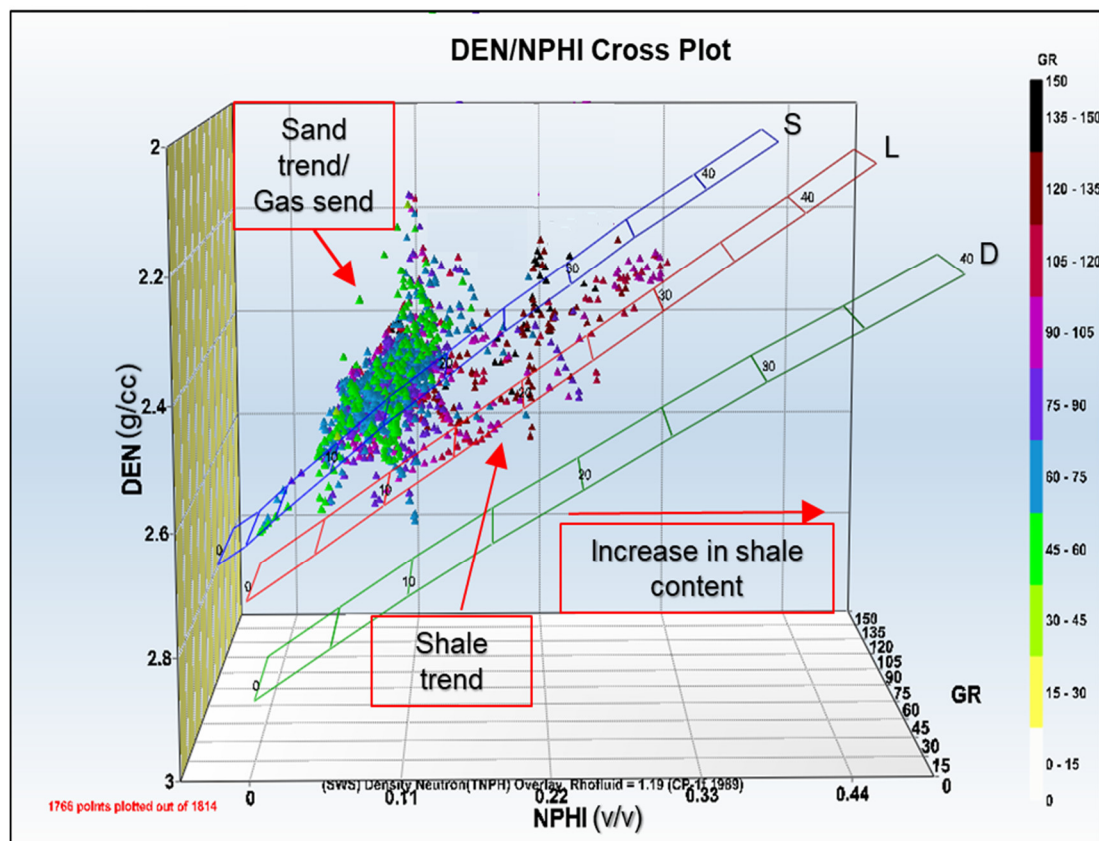


**Figure 6.** Density (RHOB)/neutron (NPHI) cross plot for multi-well analysis with discriminator gamma-ray response.



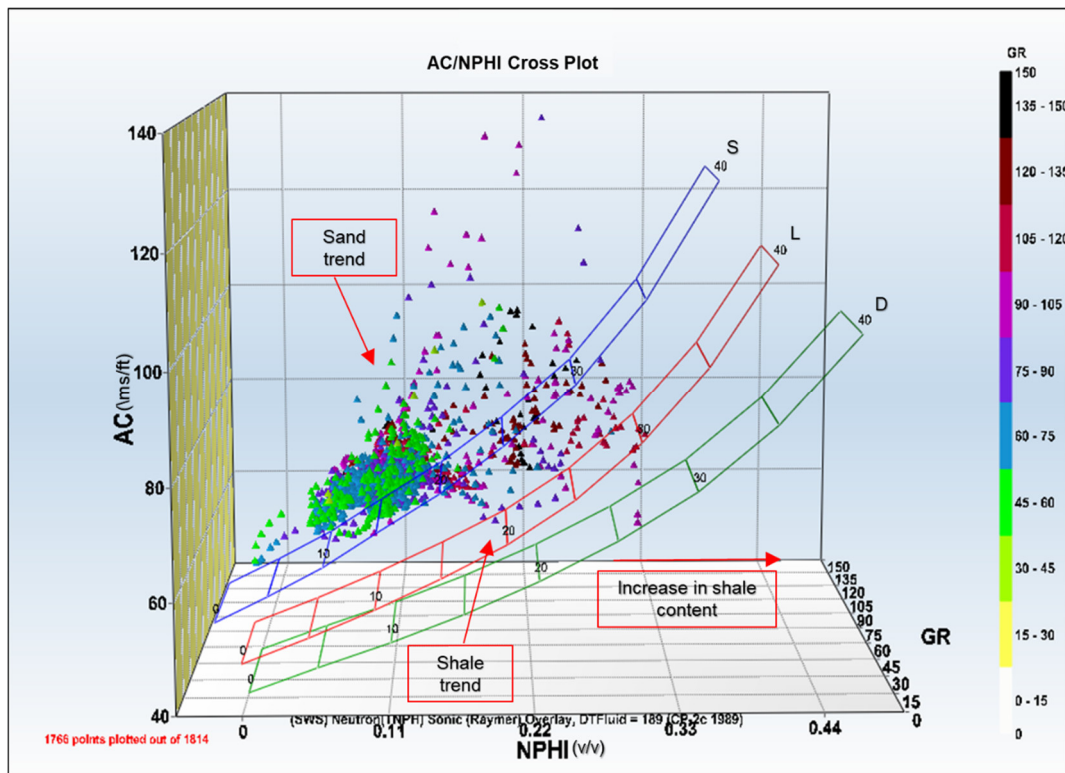


Figure 7. Neutron (NPHI)/Sonic (AC) cross plot for multi-well analysis with discriminator gamma-ray response.

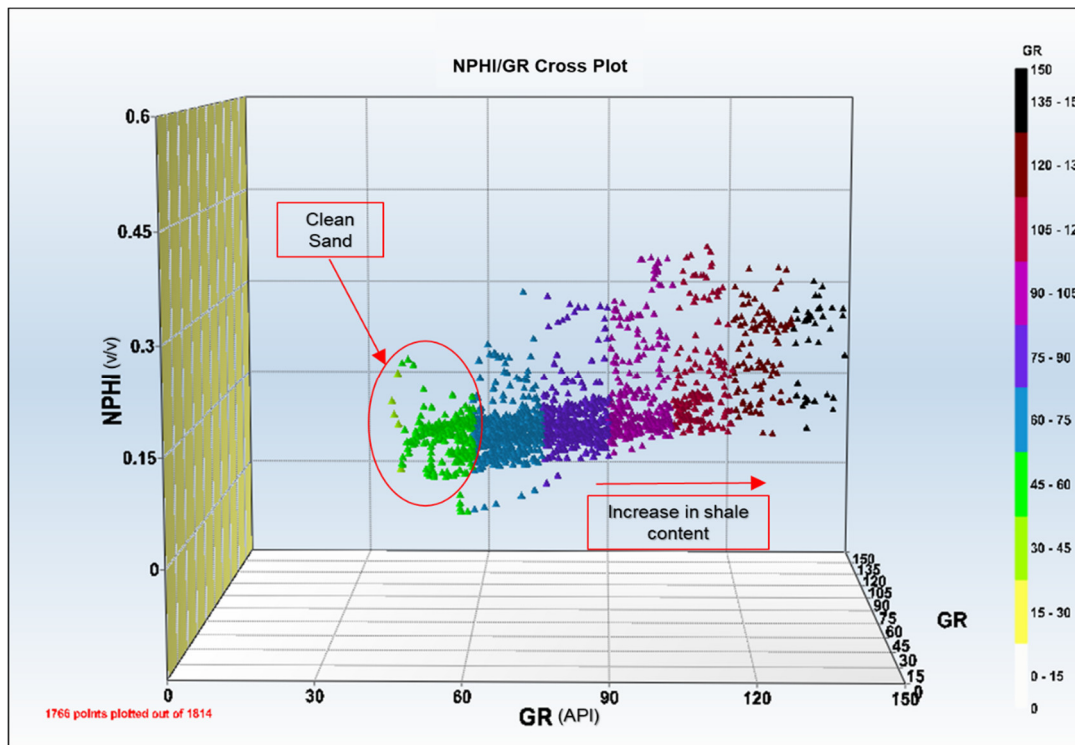


Figure 8. Neutron (NPHI)/Gamma-ray (GR) cross plot for multi-well analysis with discriminator gamma-ray response. Data falling in the black circle indicate clean sandstone.

#### 4.1.2. SOM-Based Lithofacies Evaluation

Many geological and engineering fields rely on subsurface lithofacies prediction [63]. Lithofacies can be utilized to correlate important reservoir parameters such as permeability and porosity [59,63]. The predominant task for petroleum reservoir characterization is to distinguish different lithofacies of the reservoir rocks [59,64,65].

Self-organizing maps (SOMs) are a subclass of artificial neural networks (ANNs) and have been utilized to identify lithofacies. The SOM model is suitable for visual analysis by constructing a 2D/3D view from high-dimensional to low-dimensional signal spaces and resolving reservoir heterogeneity [66–69].

Gamma ray (GR), density (DEN), neutron (NPHI), and sonic (AC) logs were employed as input data curves for the five studied wells to create the lithological section and to identify the facies variations in the reservoir interval. The results of the SOM model indicate three major lithofacies in Figures 9 and 10. The color code for each type of facies is shown as a horizontal and vertical distribution function to establish the interpreted wells' lithological description. The identified facies in the reservoir intervals demonstrate minor variations in lithological components. The facies "2" indicates pure sandstone, whereas shale/clay content is detected in the rest of the facies ("1" and "3"). The SOM model also indicates the size and hydrocarbon potential variation of the identified lithofacies. Pure sandstone demonstrates highly productive gas-bearing lithofacies, while sandstone with a minimum amount of shale/clay indicates intermediate and low gas-bearing lithofacies. It is quite convenient to obtain a first look at what the log capabilities will be in terms of group good or bad facies through this approach. The reliable results of dia-porosity cross plots and the SOM method have therefore improved lithology interpretation.

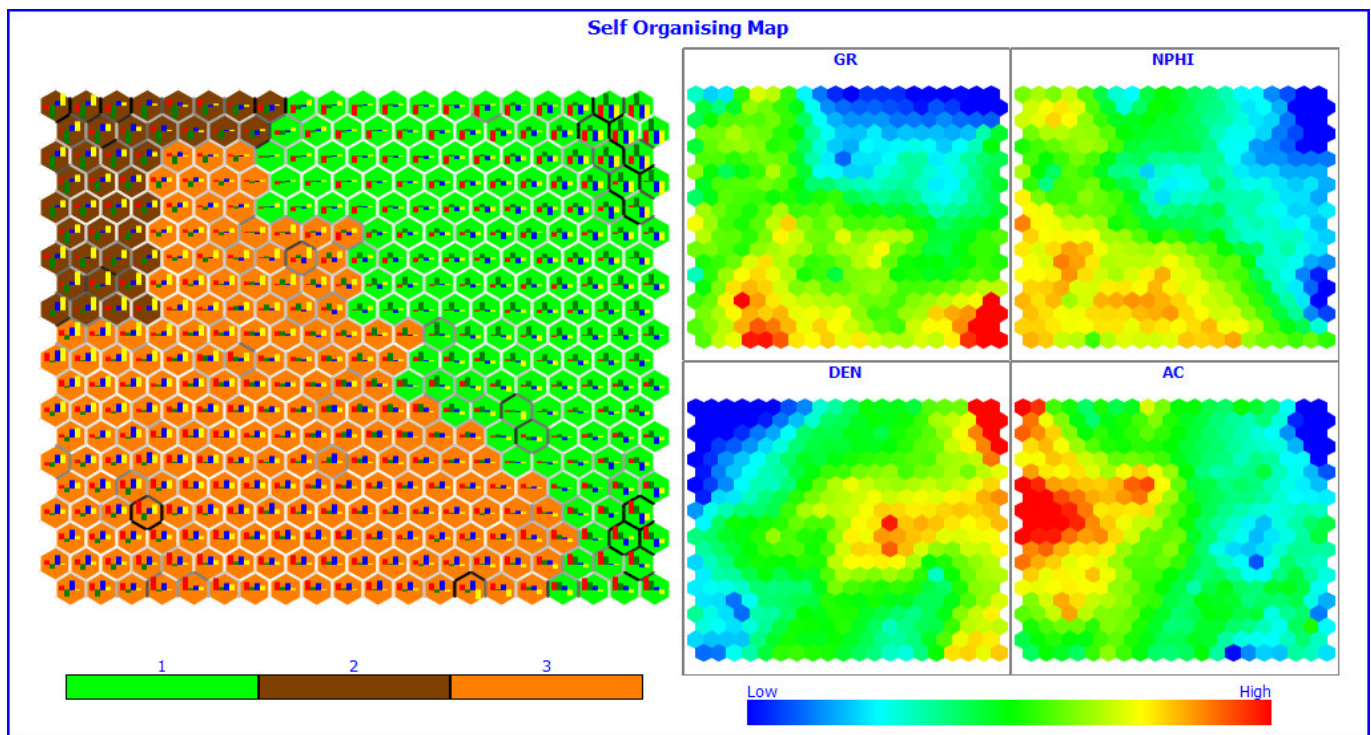


**Figure 9.** Two-dimensional facies distribution and self-organizing maps generated from gamma ray, density, acoustic, and neutron log data. Each log's contribution is indicated using a color index.

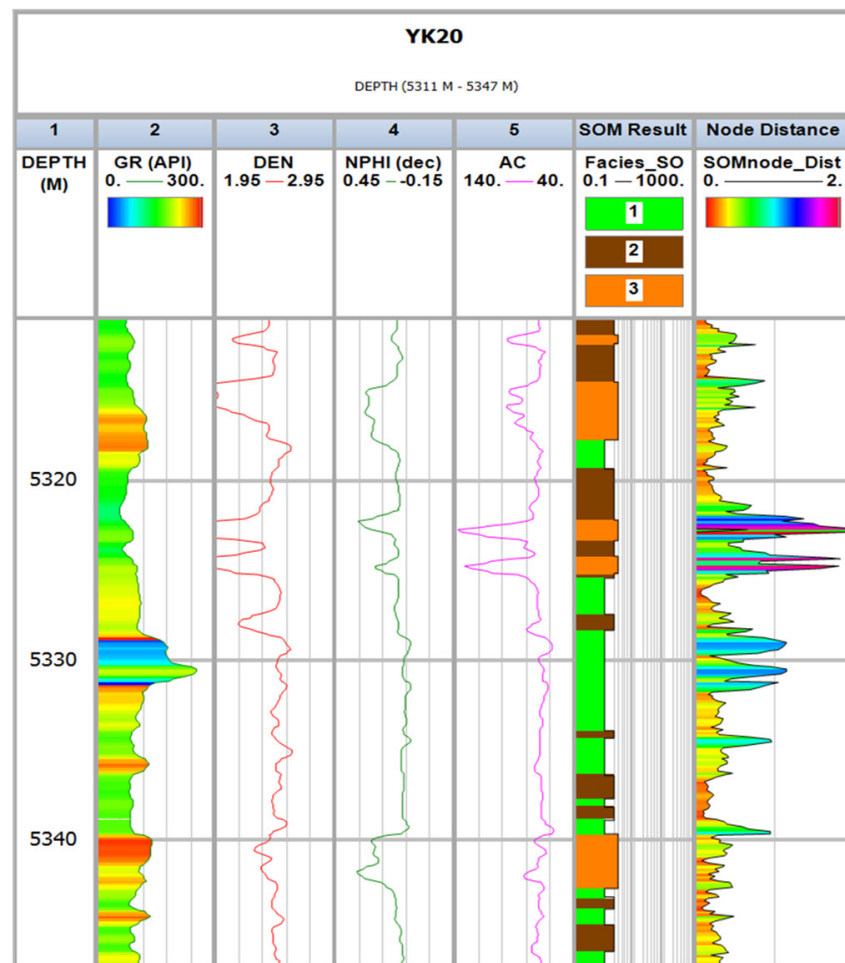


**Figure 10.** Indicating the distribution of the SOM facies vertically in reservoir intervals.

#### 4.1.3. M-N-Based Mineralogical Evaluation

The M-N cross plot is based on three porosity logs: neutron porosity, density porosity, and sonic porosity, to analyze the lithology identifiers M and N, where M is the slope on the sonic-density cross plot of the individual lithology lines and N is the slope on the neutron-density cross plot of the separate lithology lines. Data points are plotted as the triangle vertices in a ternary system triangle with the three component mineralogies. The location of each data point in the triangle indicates that particular point's mineral mixture [51,70]. It is used to distinguish the minerals, based on the porosity indicators from sonic and neutron logs, normalized by the density log [71].

The M-N plot is built for five selected wells to indicate the Cretaceous Yageliemu Formation's mineralogical components. In comparison, the tri-porosity M-N and diaporosity RHOB. vs. NPHI, AC. vs. NPHI, and GR. vs. NPHI cross plots are consistent. The M-N cross plot also confirms the abundance of clean quartzose sandstone and shows a consistent scattering of data points in Figure 11. Most of the data points are oriented quite close to the quartz sandstone position (northeast direction). In comparison, some data points are shifted slightly to the approximate shale region in a downward (southwest) direction, which indicates the reservoir rock's clastic nature. Only a few data sets allowed for the identification of secondary porosity in each well, which is facilitated by tectonic activities that result in small cracks.

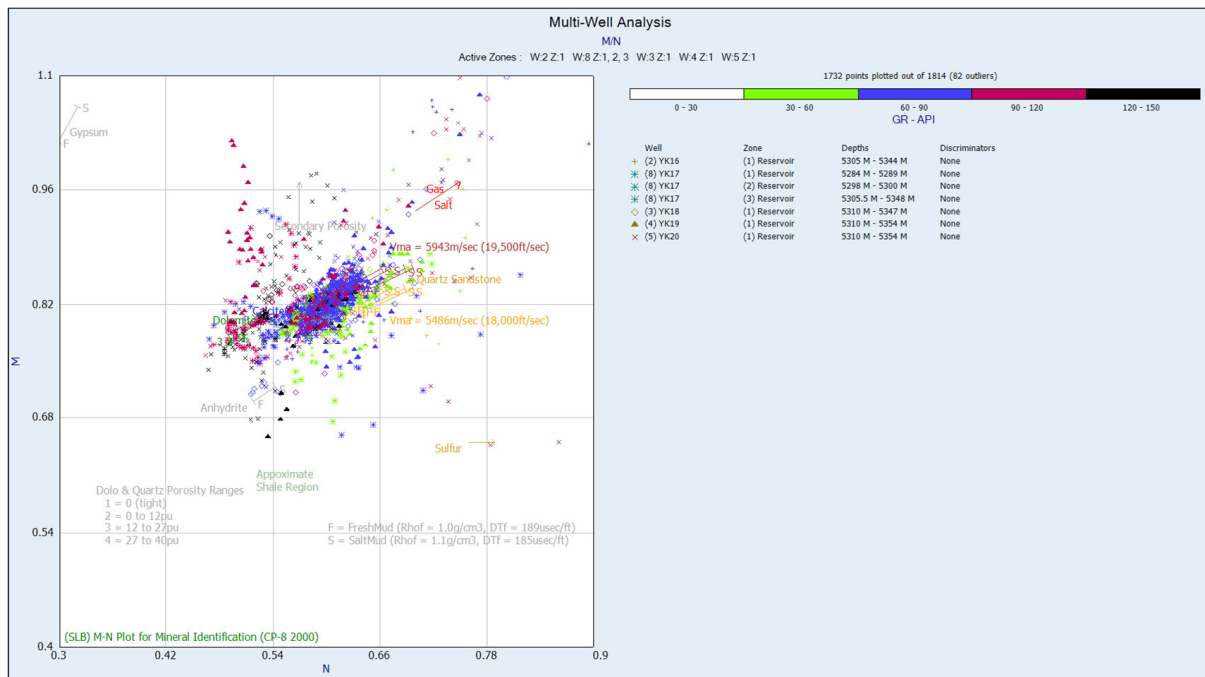


Figure 11. M-N cross plot for multi-well analysis with discriminator gamma ray response.

#### 4.2. Spatial Variations of Petrophysical Parameters

The isoperimetric 3D and color relief models of petrophysical parameters, shale content, effective porosity and permeability, water saturation, and gas saturation were built to assess the geographical variation of gas capacity in the Cretaceous Yageliemu Formation. The spatial variations of the petrophysical parameters computed for several potential zones are shown in Figures 12–16. For contouring and interpolating, average arithmetical data from several wells of the reservoir interval were posted on isoperimetric maps. The arithmetic results for all prospect zones are compiled in Table 2.

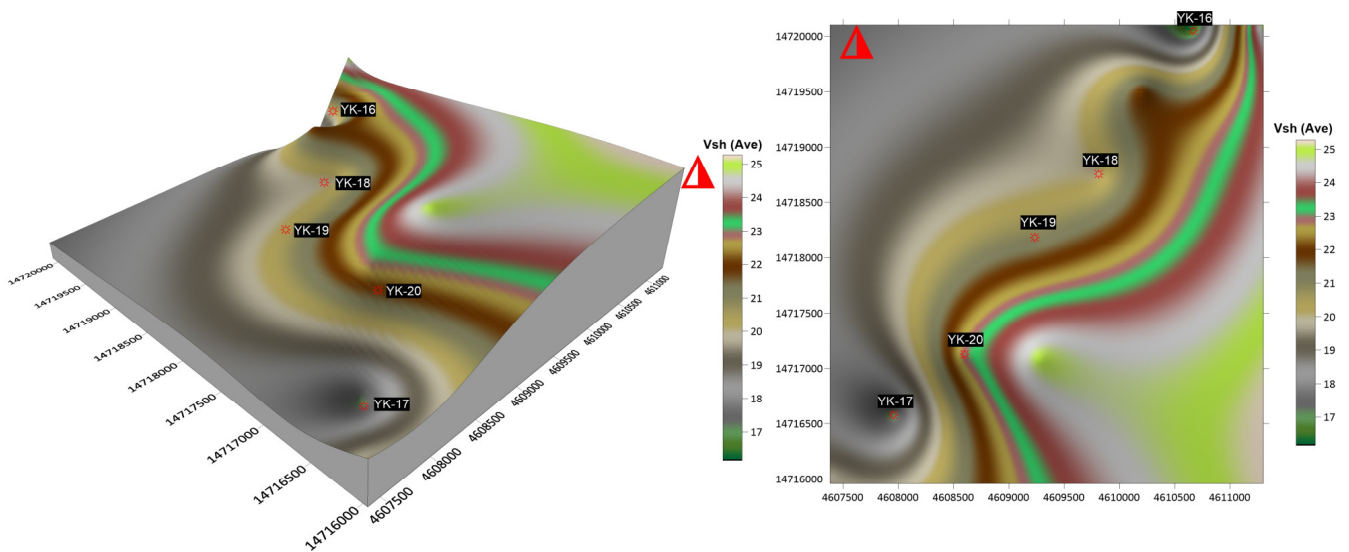


Figure 12. Shale volume variation map (calculated in %).



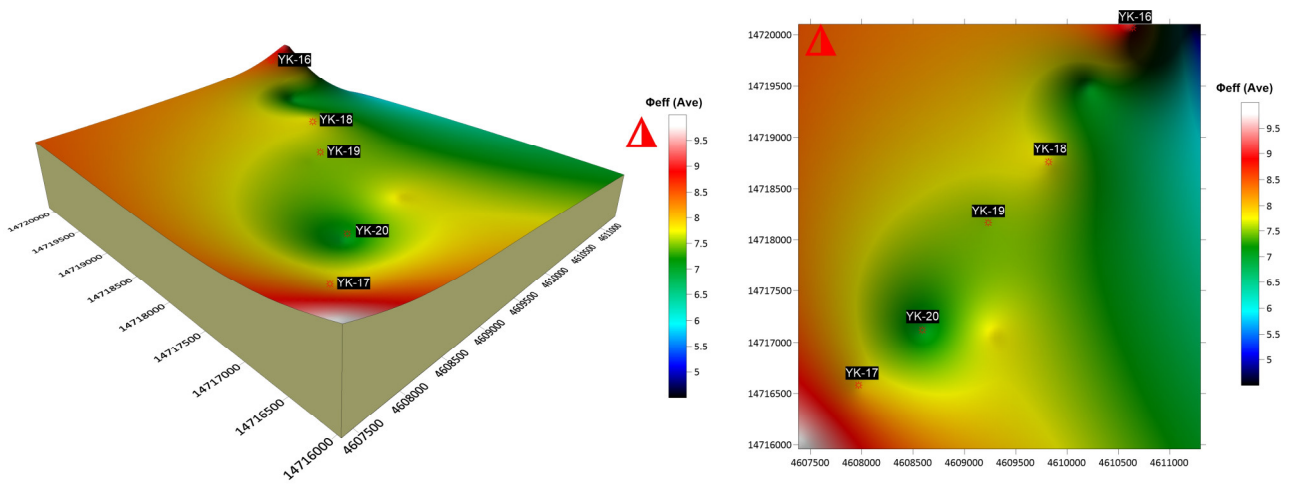


Figure 13.  $\Phi_{eff}$  map (calculated in %).

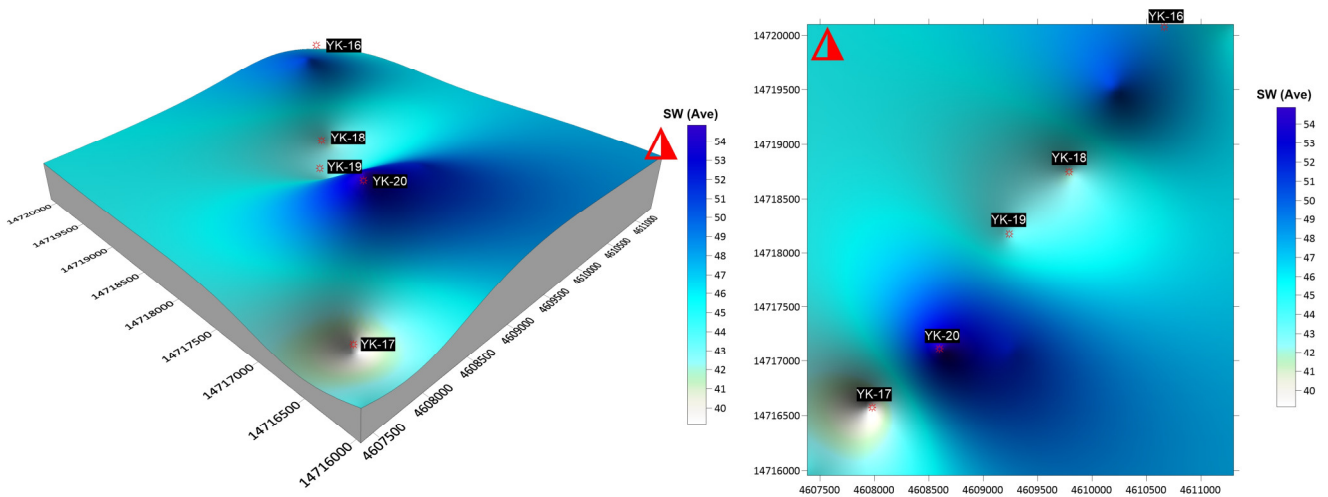


Figure 14. Water saturation ( $S_w$ ) map (calculated in %).

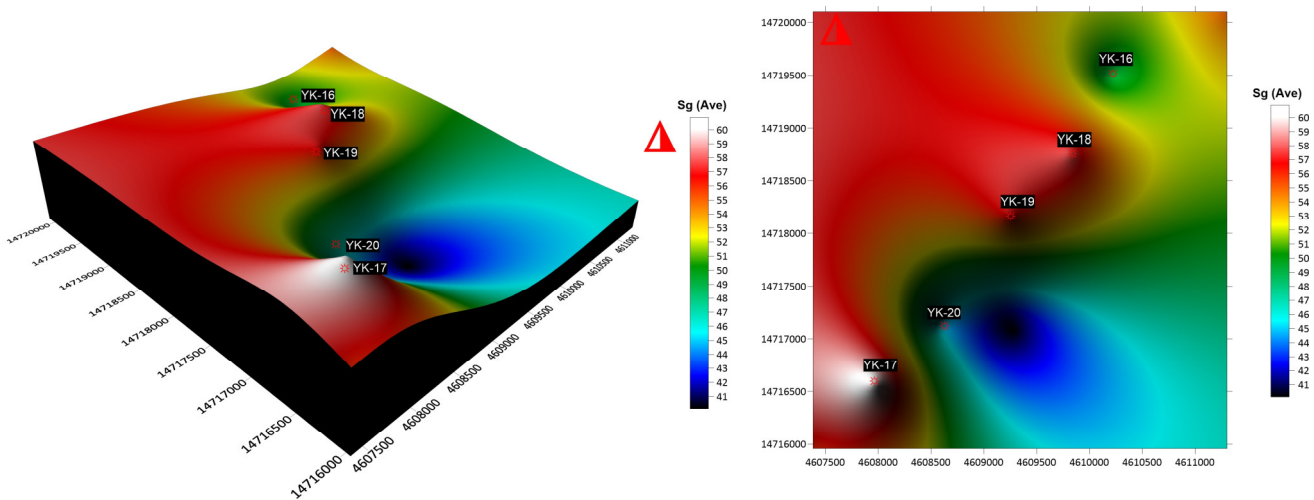


Figure 15. Gas saturation ( $S_g$ ) map (calculated in %).



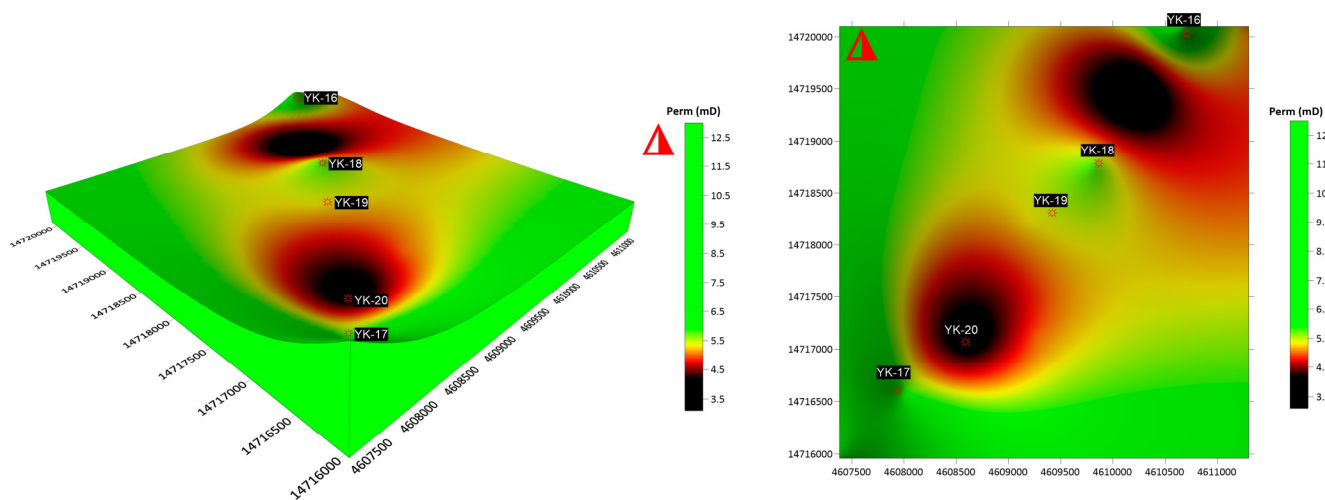


Figure 16. Permeability distribution map.

Table 2. Summary of petrophysical estimates (Ave) in proposed zones of the Yageliemu clastic reservoir.

S.No	Proposed Zone			$\Phi_{eff}$	k	Vsh	Sw	Swir	Sg
Well	Top	Bottom	Thickness(m)	%	mD	%	%	%	%
YK-16	5305	5350	45	9.2	7	16	48	43	52
YK-17	5305	5348	43	8	6	17	39	36	61
YK-18	5310	5347	37	7.8	5.8	20	42	38	58
YK-19	5310	5354	44	7.5	5.3	21	43	40	57
YK-20	5311	5347	36	7	3.7	23	55	48	45

Shale volumetric variation is an important clue for predicting the sand distribution in the study area. The lowest value of shale content is recorded at 16% in well YK16, while the highest content is detected at 23% in well YK20. A remarkable reduction in shale volume is perceived in the southwestern and northwestern parts, whereas it increases in the southeast and northeast direction of the study region.

The effective porosity’s geographic distribution map shows that the porosity varies from 7% at well YK20 to 9.2% at well YK19. The maximum value of effective porosity is found in the northwest and southeast parts of the field, while the lowest value is found in the northeastern upper, and southwestern some parts of the study region. This might indicate the modification of porosity of rock with geological time and depositional environment into the rock which influences the porosity deficiency or vice versa.

The water saturation distribution map indicates that Sw’s maximum presence is assessed within the range of 55% in well YK20 and 39% in well YK17. The Sw tends to increase towards the northeast and southeast portion of the study area, while the decrease can be seen in water saturation content towards the northwest and southwest parts of the Cretaceous Yageliemu Formation.

The gas saturation distribution map of the selected reservoir zones varies from 45% in well YK20 to 61% in well YK17. Sg high saturation closures are found in the northwest and southwest parts of the field. Previous research also indicates that petroleum was observed moving toward the northwest and accumulating at the structural high [72]. In contrast, Sg saturation tends to decrease in the northeast and southeast direction of the research area.

Based on the permeability distribution pattern, we can see that the K value ranges from 3.7 mD at well YK20 to 7 mD at well YK16. The permeability distribution map displays a closure with high permeability in the northwestern and southwestern portions of the field, except for the area covered by YK20. While a permeability reduction is noticed in the northeast direction, it is outgoing from east to the south, and the permeability values first tend to decrease before a remarkable rise is observed.

#### 4.3. Well Correlation

The identification and linking of related patterns and/or values between log curves of nearby wells are known as well log correlation. Good or correct correlation is almost like an acquired skill or craft; therefore, there is often significant argument and disagreement about the outcomes. The accurate correlation of multiple characteristics or patterns on several or more well logs might produce surfaces that collectively build the subsurface feature template.

Figure 17 shows the correlation between all five wells in the present study. The gamma ray was the well-log parameter used in the correlation. The purpose of using these correlation logs is that they have been linked to petrophysical properties. In other words, their log scale behavior is tied to the formation property's behavior. The well correlation also shows the vertical distribution of effective porosity, permeability, gas saturation, water saturation, and sand shale volume in each well and has a good correlation.

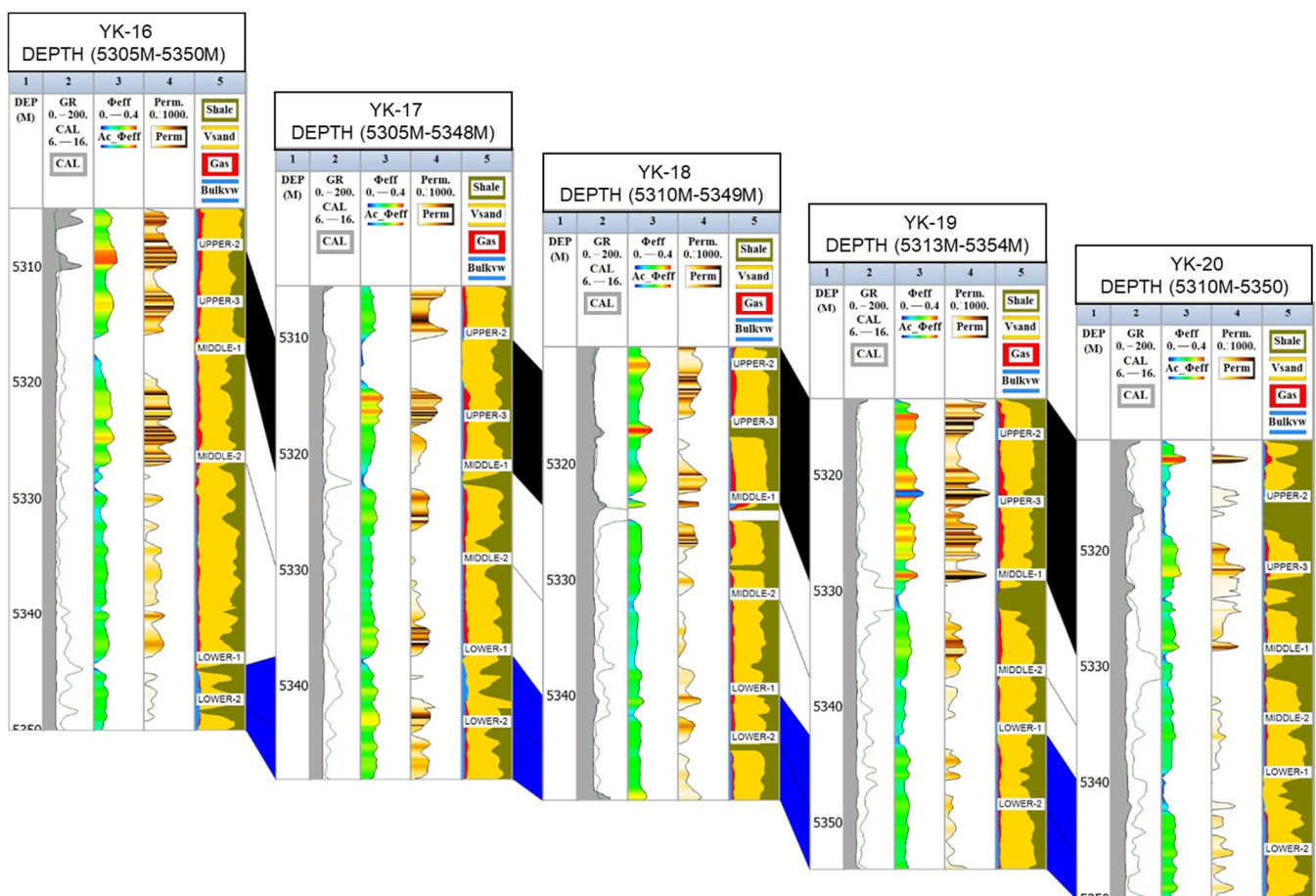


**Figure 17.** Vertical distribution of predicted petrophysical properties for each well in the analyzed field's gas layers (permeability, effective porosity, bulk water volume, gas saturation, and sand and shale volume).

#### 4.4. Pickett Plot

A Pickett plot was interpolated for the determination of water saturation ( $S_w$ ). The Pickett plot also denominated porosity resistivity, which is an ideal graphical solution to the Archie equation [49–51]. Furthermore, several essential factors, including tortuosity factor, cementation exponent, and saturation exponent ( $a$ ,  $m$ ,  $n$ , respectively), were also determined for the studied area. In addition, for water resistivity ( $R_w$ ) values, the SP approach was used, which is a very useful method for calculating  $R_w$  values over many zones. The findings of these essential parameters are shown in Table 3. The Cretaceous Yageliemu For-

mation Pickett plot results are shown in Figure 18. A fluid mixture (hydrocarbon-bearing “H/C” and water-bearing “Sw” data points) is distinctly indicated. Some clusters are plotted beneath the 100% water saturation (Sw) line, which means a 100% water-bearing zone. An effective indication of gas-bearing zones is found when the cluster position moved in the northeast direction. In contrast, the water saturation line reduction occurred from 50% to 20% (In the dwindling sequence of the effective porosity log). A reasonable match between the plotting results and gamma ray values is observed (See the Z-axis color code at the bottom of the Pickett plot).

**Table 3.** Archie parameters for the research area.

Well ID	a	m	n	Rw
YK-16	0.65	1.80	2	0.035
YK-17	0.65	1.90	2	0.030
YK-18	0.65	1.80	2	0.034
YK-19	0.65	1.80	2	0.035
YK-20	0.65	1.80	2	0.035

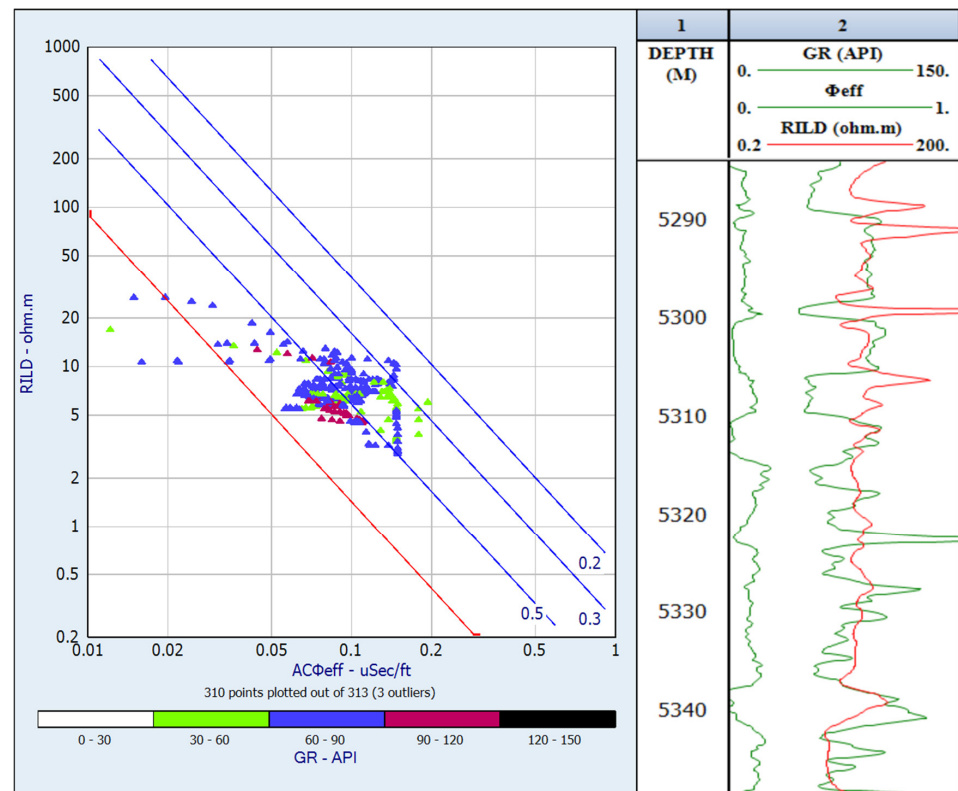


**Figure 18.** Pickett plots (RILD/Ac\_Φeff cross plot) for YK-16 with discriminator gamma ray response.

#### 4.5. Irreducible Water Saturation (Swir)

Irreducible water saturation (Swir) is an important parameter for predicting relative permeability and estimating initial natural gas reserves. The Swir for Yageliemu Formation sands indicates a reasonable match with water saturation values. It has been noticed that irreducible water saturation increases when water saturation rises. The values of irreducible water saturation for each well are shown in Table 2. These Swir values are used as input in the permeability calculations.

#### 4.6. Shale Structure

The presence of shale in zones of interest can decrease reservoir productivity because shale reduces the reservoir’s effective porosity and permeability [73–77]. Therefore, the distribution of shale in reservoir rock cannot be neglected as it may have a considerable impact on the capacity to accurately estimate reservoir hydrocarbon reserves. As such, incorrect estimates of hydrocarbons’ potential will result in missed opportunities for the extraction of more hydrocarbons [78]. That is why shale volume quantification is one of the vital essential influences to consider in reservoir assessment, particularly in shaly sand sequences, which is highly important. The types of shale distribution are defined as dispersed shale, laminar shale, and structural shale, or shaly material can take place within a reservoir in any number of combinations [79–81]

Thomas and Stieber were the first to formalize and describe the shale distribution types [82] and categorize the type of shales as laminar, dispersed, and structural, and noted their impact on reservoir properties. Shale distribution types in identified sand packages of the Cretaceous Yageliemu Formation have been determined based on the Thomas–Stieber model which is indicated in Figure 19. Based on the data plotting positions in the cross plot, the dispersed and laminated shale volumes in the sand bodies can be distinguished and acknowledged.

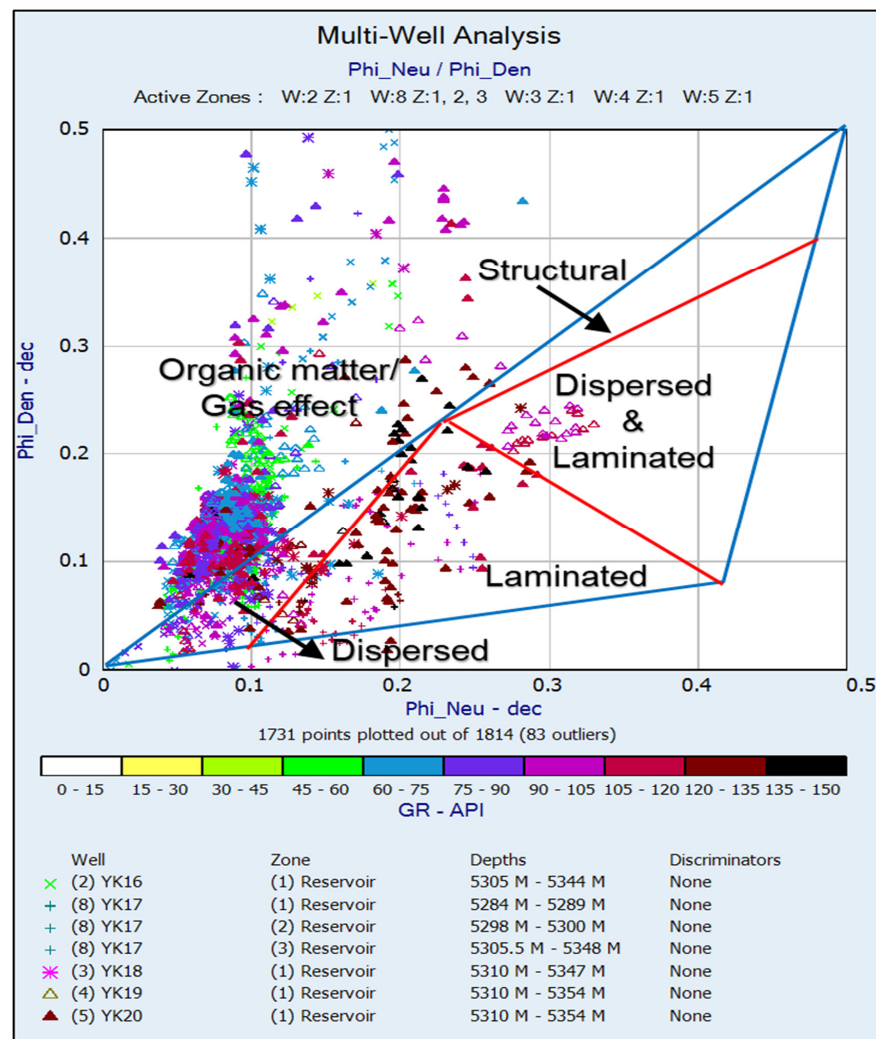


**Figure 19.** Phi Den/Phi Neu cross plot for multi-well analysis with a discriminator gamma ray. The response indicates the shale distribution types in reservoir intervals.

Laminar shale is present in some quantities in the sand bodies, as thin layers of allogeneic clay that has no impact on water saturation, effective porosity, or horizontal reservoir sand bodies permeability; however, the vertical permeability of reservoir sand bodies is influenced. The study reveals that sand bodies are composed of a little amount of dispersed shale but no structural shale. The distribution of the dispersed shale type in sand influences the quality of reservoir sand bodies. The effect may be increased water saturation (as shale water wetness is usually more significant than sand) and reduced porosity (as dispersive shale fills pore spaces) [83]. Structural shale has characteristics similar to laminated shale, but its resistivity permeability and characteristics are the same as the dispersive shale characteristics. Therefore, the presence of a minor volume of dispersive shale and the absence of structural shale suggests that the sand bodies have adequate reservoir consistency.

#### 4.7. Reservoir Rock Typing

The rock types reflect reservoir bodies with a distinct link between effective porosity, deliverability, hydrocarbon storage potential, and appropriate water saturation level [79,80,83–85]. It leads to an excellent perception of reservoir fluid and oil recovery [86]. The potential to hold hydrocarbons is characterized by the effective porosity, while the deliverability depends on the permeability. The current effective porosity ability to contribute to permeability is referred to as the reservoir quality index (RQI) [87–90].

The reservoir rock typing quality of the identified sand bodies is tested using a cluster analysis approach. The gamma ray log (GR), effective porosity (PHIE), effective permeability (K), and water saturation (SW) logs for five studied wells were used as input data for cluster analysis, and four clusters are supposed to cover all data variations as shown in well histograms. Each facies is described by the mean values of input data curves. The “cluster mean” results of each well are presented in Table 4, which displays the mean values and additional statistics for each cluster (four clusters) of the utilized data. Upon categorizing the used data into four clusters, groups of log facies were generated from these clusters. The Cretaceous Yageliemu Formation log facies of each well were divided into four groups. Each log facies group was interpreted to evaluate the reservoir parameters (effective porosity, effective permeability, and water saturation). Based on the cluster analysis, log facies 1 and 2 are the most important zones in the Yageliemu clastic reservoir. The cross plots and histograms between the input data curves can be seen in Figure 20, which was built with the use of k means cluster evaluation for the facies groups. The reservoir rock typing properties of the log facies are shown in Table 5.

**Table 4.** Results of cluster assessment for each rock type.

K-Mean Clustering Results										
Facies	Points	Rock Typing	GR Mean/Std Dev		$\Phi_{eff}$ Mean/Std Dev		Perm Mean/Std Dev		Sw Mean/Std Dev	
1	342	Excellent	63	11	0.13	0.016	13	8	0.33	0.06
2	934	Good	84	22	0.09	0.015	3	3.53	0.52	0.10
3	383	Moderate	108	55	0.035	0.025	0.037	0.09	0.93	0.091
4	48	Poor	124	136	0.02	0.018	0.004	0.011	0.99	0.024

**Table 5.** The properties of log facies.

Facies. No	Rock Typing	GR	$\Phi_{eff}$	Perm	Sw
Facies-01	Excellent quality rock type	Very low	Good to excellent	Good to excellent	Very low
Facies-02	Good quality rock type	Low	Good	Good	Low
Facies-03	Moderate quality rock type	Medium	Fair to good	Fair to good	Medium
Facies-04	Poor quality rock type	High	Low	Low	Very high



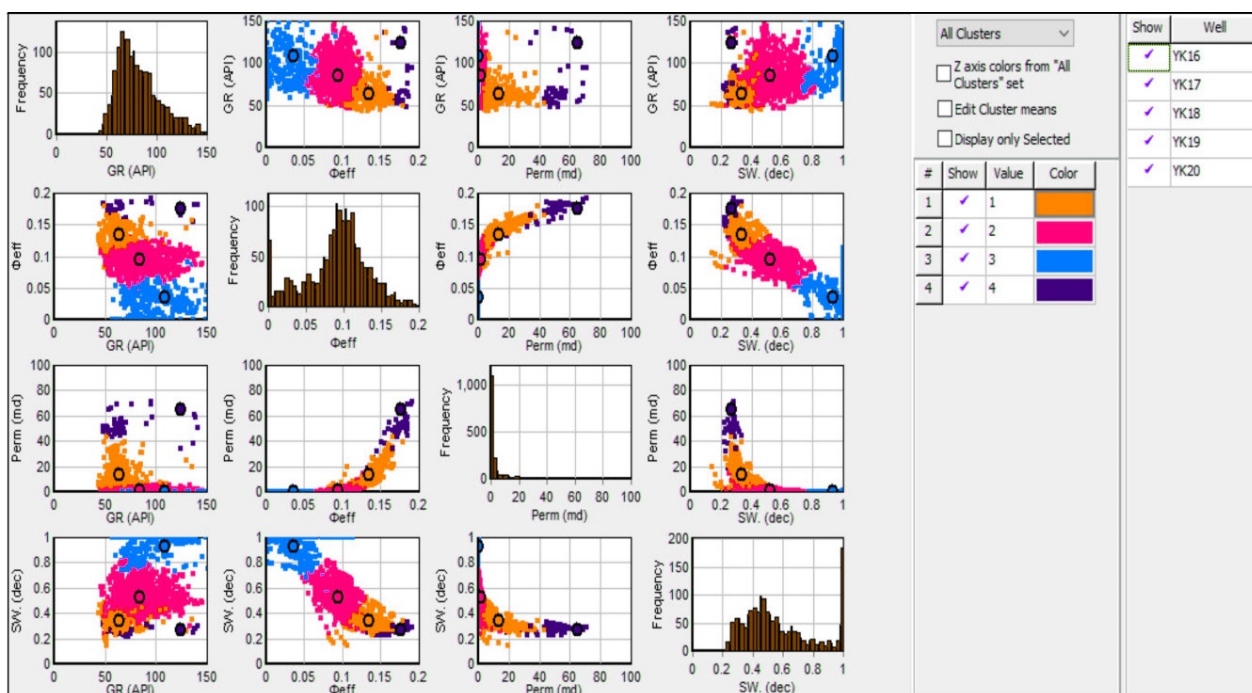


Figure 20. The final graphical results of the clustering assessment.

## 5. Conclusions

The petrophysical evaluation identifies the hydrocarbon prospects of the Yageliemu Formation, which is comprised of wire-line log investigations that focus on pre-established calculations/formulas, cross plots, and charts. Based on these results, the following conclusions can be drawn:

The density log and neutron log data for petrophysical logs are unreliable because some zones are affected by borehole anomalies (washout/breakout). Therefore, the sonic log was used to evaluate porosity.

We concluded from the cross plot assessment that the lithological description of the reservoirs of the Yageliemu Formation is thick porous sandstone with some shale intercalations. Furthermore, the Thomas–Stieber model revealed that the zones of interest had sufficient reservoir consistency due to a low fraction of dispersive shale and a lack of structural shale.

Cluster analysis of log data of each well indicates that the reservoir rock typing quality of the present research can be divided into four distinct groups of log facies. The results reveal that the most interesting zones of the Yageliemu clastic reservoir for the YKL gas field are log facies 1 and 2.

In all wells of the Pickett plot matching, a remarkable similarity was observed. Three factors ( $a$ ,  $m$ , and  $n$ ) were determined for reservoir salinity and water resistivity formation via this well matching. For  $a$ ,  $n$ , and  $m$ , similar estimated values were revealed. In the interpretation of well logs, these values were utilized. A rigorous procedure was employed in the water saturation method to compute the ( $a$ ,  $m$ , and  $n$ ) values since erroneous values can overestimate/underestimate the extractable interest zone.

The petrophysical analysis of the study area revealed a prolific gas zone. The assessment of petrophysical parameters characterized the reservoir zones of each well (average water saturation (SW) ranging from 39 to 56%; average gas saturation (Sg) ranging from 45 to 61%; average permeabilities (K) ranging from 3.7 mD to 7 mD; average effective porosities ( $\Phi_{eff}$ ) ranging from 7 to 9.2%).

The isochore map indicates that additional boreholes could be drilled in the southwest and northwest areas of the research region. It is suggested that the southeastern and north-

eastern parts of the research area should be avoided due to the high water concentration and rise in the volume of shale. Furthermore, determining the optimum cost-effective technique of producing hydrocarbons from the present study gas field wells should not be dependent primarily on the responses of geophysical logs; additionally, scientific proof acquired from a range of reservoir evaluation methodologies should be considered.

**Author Contributions:** W.H. conceived this study. L.P. and X.W. supervised this project. S.C., H.L., and L.L. provided the data. W.H. and M.A. prepared the original draft along with software analysis. S.U.D., H.H. and A.J. completed the writing—review and editing. M.E. reviewed the manuscript and provided the necessary funding. All the authors discussed the results and contributed to the final manuscript. All authors have read and agreed to the published version of the manuscript.

**Funding:** M.E. provided the necessary funding.

**Data Availability Statement:** Data available on request due to privacy/ethical restrictions.

**Acknowledgments:** The authors would like to thank the fluid flow lab of the Faculty of Earth Resources China University of Geosciences for their cooperation in completing this research.

**Conflicts of Interest:** The authors declare that they have no known competing financial interest or personal relationships that might have influenced the work presented in this article.

## Nomenclature

YKL	Yakela (gas field name)
YK16	Yakela16 (well name)
YK17	Yakela17 (well name)
YK18	Yakela18 (well name)
YK19	Yakela19 (well name)
YK20	Yakela20 (well name)

## References

1. Pigott, J.D.; Williams, M.T.; Abdel-Fattah, M.; Pigott, K.L. The Messinian Mediterranean Crisis: A Model for the Permian Delaware Basin? In Proceedings of the AAPG international conference and exhibition, Istanbul, Turkey, 14–17 September 2014.
2. Ali, M.; Khan, M.J.; Ali, M.; Iftikhar, S. Petrophysical analysis of well logs for reservoir evaluation: A case study of “Kadanwari” gas field, middle Indus basin, Pakistan. *Arab. J. Geosci.* **2019**, *12*, 215.
3. Ali, M.; Ma, H.; Pan, H.; Ashraf, U.; Jiang, R. Building a rock physics model for the formation evaluation of the Lower Goru sand reservoir of the Southern Indus Basin in Pakistan. *J. Pet. Sci. Eng.* **2020**, *194*, 107461. [[CrossRef](#)]
4. Ali, N.; Chen, J.; Fu, X.; Hussain, W.; Ali, M.; Iqbal, S.M.; Anees, A.; Hussain, M.; Rashid, M.; Thanh, H.V. Classification of reservoir quality using unsupervised machine learning and cluster analysis: Example from Kadanwari gas field, SE Pakistan. *Geosyst. Geoenviron.* **2022**, *2*, 100123.
5. Hussain, W.; Ali, N.; Sadaf, R.; Hu, C.; Nykilla, E.E.; Ullah, A.; Iqbal, S.M.; Hussain, A.; Hussain, S. Petrophysical analysis and hydrocarbon potential of the Lower Cretaceous Yageliemu Formation in Yakela gas condensate field, Tarim Basin, China. *Geosyst. Geoenviron.* **2022**, *1*, 100106.
6. Abdel-Fattah, M.I.; Metwalli, F.I.; El Sayed, I.M. Static reservoir modeling of the Bahariya reservoirs for the oilfields development in South Umbarka area, Western Desert, Egypt. *J. African Earth Sci.* **2018**, *138*, 1–13. [[CrossRef](#)]
7. Chongwain, G.M.; Osinowo, O.O.; Ntamak-Nida, M.J.; Nkoa, E.N. Seismic Attribute Analysis for Reservoir Description and Characterization of M-Field, Douala Sub-Basin, Cameroon. *Adv. Pet. Explor. Dev.* **2017**, *15*, 1–10.
8. Ellis, D.V.; Singer, J.M. *Well Logging for Earth Scientists*; Springer: Berlin/Heidelberg, Germany, 2007; Volume 692.
9. Naem, M.; Jafri, M.K.; Moustafa, S.S.R.; AL-Arifi, N.S.; Asim, S.; Khan, F.; Ahmed, N. Seismic and well log driven structural and petrophysical analysis of the Lower Goru Formation in the Lower Indus Basin, Pakistan. *Geosci. J.* **2016**, *20*, 57–75. [[CrossRef](#)]
10. Qiao, Y.; An, H. Study of petrophysical parameter sensitivity from well log data. *Appl. Geophys.* **2007**, *4*, 282–287. [[CrossRef](#)]
11. Rashid, M.; Luo, M.; Ashraf, U.; Hussain, W.; Ali, N.; Rahman, N.; Hussain, S.; Aleksandrovich Martyushev, D.; Vo Thanh, H.; Anees, A. Reservoir quality prediction of gas-bearing carbonate sediments in the Qadirpur Field: Insights from advanced machine learning approaches of SOM and cluster analysis. *Minerals* **2023**, *13*, 29. [[CrossRef](#)]
12. Bachrach, R.; Beller, M.; Liu, C.C.; Perdomo, J.; Shelander, D.; Dutta, N.; Benabentos, M. Combining rock physics analysis, full waveform prestack inversion and high-resolution seismic interpretation to map lithology units in deep water: A Gulf of Mexico case study. *Lead. Edge* **2004**, *23*, 378–383. [[CrossRef](#)]

13. Gommesen, L.; Hansen, H.P.; Pedersen, J.M.; Marsden, G.; Schiott, C.R. Rock physics templates and seismic modelling of chalk reservoirs in the South Arne Field of the Danish North Sea. In Proceedings of the Extended Abstract G019 Presented at 66th EAGE Technical Conference & Exhibition, Paris, France, 7–10 June 2004.
14. Ajisafe, Y.C.; Ako, B.D. 3-D seismic attributes for reservoir characterization of “Y” field Niger Delta, Nigeria. *IOSR J. Appl. Geol. Geophys.* **2013**, *1*, 23–31.
15. Nabawy, B.S.; El Sharawy, M.S. Reservoir assessment and quality discrimination of Kareem Formation using integrated petrophysical data, Southern Gulf of Suez, Egypt. *Mar. Pet. Geol.* **2018**, *93*, 230–246. [[CrossRef](#)]
16. Fawad, N.; Liu, T.; Fan, D.; Ahmad, Q.A. Sedimentary Facies Analysis of the Third Eocene Member of Shahejie Formation in the Bonan Sag of Bohai Bay Basin (China): Implications for Facies Heterogeneities in Sandstone Reservoirs. *Energies* **2022**, *15*, 6168. [[CrossRef](#)]
17. Abdel-Fattah, M.I. Impact of depositional environment on petrophysical reservoir characteristics in Obaiyed Field, Western Desert, Egypt. *Arab. J. Geosci.* **2015**, *8*, 9301–9314. [[CrossRef](#)]
18. Nabawy, B.S.; Géraud, Y. Impacts of pore-and petro-fabrics, mineral composition and diagenetic history on the bulk thermal conductivity of sandstones. *J. Afr. Earth Sci.* **2016**, *115*, 48–62. [[CrossRef](#)]
19. Ahmad, Q.A.; Ehsan, M.I.; Khan, N.; Majeed, A.; Zeeshan, A.; Ahmad, R.; Noori, F.M. Numerical simulation and modeling of a poroelastic media for detection and discrimination of geo-fluids using finite difference method. *Alex. Eng. J.* **2022**, *61*, 3447–3462. [[CrossRef](#)]
20. Orji, C.S.; Uko, E.D.; Tamunobereton-ari, I. Permeability-Porosity Trends In Cawc Reservoir Sands In The Niger Delta Nigeria, Using Well-Log Data. *Malays. J. Geosci.* **2019**, *3*, 33–42. [[CrossRef](#)]
21. Liu, T.; Fawad, N.; Li, C.; Li, H.; He, R.; Xu, J.; Ahmad, Q.A. Physical simulation of remaining oil distribution in the 3rd-order architecture unit in beach sand reservoir. *Front. Earth Sci.* **2023**, *10*, 1108525. [[CrossRef](#)]
22. Tang, J.; Yin, H.; Wang, G.; Chen, Y. Methane microseepage from different sectors of the Yakela condensed gas field in Tarim Basin, Xinjiang, China. *Appl. Geochem.* **2010**, *25*, 1257–1264. [[CrossRef](#)]
23. Junhong, T.; Zhengyu, B.; Xiang, W.; Qinghong, G. Geological emission of methane from the Yakela condensed oil/gas field in Talimu Basin, Xinjiang, China. *J. Environ. Sci.* **2008**, *20*, 1055–1062.
24. Geng, Y.; Li, J.; He, D. Trap types, distribution and the law of spatial combination in the west Tabei uplift, Tarim Basin. *ACTA Sci. Nat. Pekin.* **2008**, *44*, 193.
25. Xiuxiang, L.; Jianjiao, L.; Fengyun, Z.; Ning, Y.; Qiucha, Z. North-south Differentiation of the Hydrocarbon Accumulation Pattern of Carbonate Reservoirs in the Yingmaili Low Uplift, Tarim Basin, Northwest China. *Acta Geol. Sin. Ed.* **2008**, *82*, 499–508. [[CrossRef](#)]
26. Luo, X.L.; Tang, L.J.; Xie, D.Q.; Qiu, H.J.; Jiang, H.S.; Yang, Y.; Chen, X.Y.; Zhang, Y.H. Strike-slip movement and its genetic mechanism in Yakela faulted salient, the Tarim Basin. *Oil Gas Geol.* **2013**, *34*, 257–263.
27. Li, M.; Wang, T.-G.; Li, H.; Fang, R.; Yang, L.; Shi, S.; Kuang, J. Occurrence and geochemical significance of phenylnaphthalenes and terphenyls in oils and condensates from the Yakela Faulted Uplift, Tarim Basin, Northwest China. *Energy Fuels* **2016**, *30*, 4457–4466. [[CrossRef](#)]
28. Song, D.; Wang, T.-G.; Li, H. Geochemical characteristics and origin of the crude oils and condensates from Yakela Faulted-Uplift, Tarim Basin. *J. Pet. Sci. Eng.* **2015**, *133*, 602–611. [[CrossRef](#)]
29. Huiling, Y. Analysis of structural patterns and evolution characteristics in south Tianshan area. *Geophys. Prospect. Pet.* **2008**, *15*, 277–284.
30. Luo, X.L.; Tang, L.J.; Xie, D.Q.; Qiu, H.J.; Jiang, H.S.; Yang, Y.; Chen, X.Y.; Zhang, Y.H. Structural styles and hydrocarbon accumulation in Yakela fault-convex, Tarim Basin. *Pet. Geol. Recov. Effic.* **2012**, *19*, 38–41.
31. Ren-bing, G. Characteristics of Stratigraphic Pressure in the Middle Yakela Fault Block. *West China Pet. Geosci.* **2005**, *1*, 77–84.
32. Jarrett, K.; Kavukcuoglu, K.; Ranzato, M.; LeCun, Y. What is the best multi-stage architecture for object recognition? In Proceedings of the 2009 IEEE 12th International Conference on Computer Vision, Kyoto, Japan, 29 September–2 October 2009; pp. 2146–2153.
33. Yang, C.L.; Wu, Q.Z.; Xia, Y.P. The origin of Mesozoic–Cenozoic extension-tensional fault system in the North Positive Element in the Tarim Basin, and its role in accumulating oil and gas. *Oil Geophys. Prospect.* **2000**, *35*, 461–468.
34. Wei, G. Tectonic characteristics and petroleum accumulation in extensional-shear fault system in Mesozoic–Cenozoic formations in the northern area of Tabei Uplift, Tarim. *Acta Pet. Sin.* **2001**, *22*, 19–24.
35. Zhou, X.; Sun, B.; Xu, H. Tectonic Deformation of Yakerla-Luntai Region in North Tarim Basin and Its Control on Oil/Gas Accumulation. *J. Geomech.* **2001**, *7*, 33–40.
36. Xu, K.; Tian, J.; Yang, H.; Zhang, H.; Ju, W.; Liu, X.; Wang, Z.; Fang, L. Effects and practical applications of present-day in-situ stress on reservoir quality in ultra-deep layers of Kuqa Depression, Tarim Basin, China. *J. Nat. Gas Geosci.* **2022**, *7*, 85–94. [[CrossRef](#)]
37. Huang, C.; Yang, B.; Zhao, X.-S. Log interpretation of reservoir parameters and reservoir evaluation for yageliemuzu formation in yakela gasfield. *Xinjiang Oil Gas* **2010**, *4*, 9-14, 26+117.
38. Qiang, Y. Reservoir comprehensive classification and evaluation research of Yageliemu formation in YK gas reservoir. *Pet. Geol. Eng.* **2012**, *26*, 71–74+8.
39. Rider, M.H.; Kennedy, M. *The Geological Interpretation of Well Logs*, 2nd ed.; Rider-French Consulting: Southerland, UK, 2002; 280p.

40. Clavier, C.; Hoyle, W.; Meunier, D. Quantitative interpretation of thermal neutron decay time logs: Part I. Fundamentals and techniques. *J. Pet. Technol.* **1971**, *23*, 743–755. [[CrossRef](#)]
41. Azeem, T.; Chun, W.Y.; Khalid, P.; Qing, L.X.; Ehsan, M.I.; Munawar, M.J.; Wei, X. An integrated petrophysical and rock physics analysis to improve reservoir characterization of Cretaceous sand intervals in Middle Indus Basin, Pakistan. *J. Geophys. Eng.* **2017**, *14*, 212–225. [[CrossRef](#)]
42. Atlas, W. *Introduction to Wireline Log Analysis*; West Atlas Int Inc.: Houston, TX, USA, 1995.
43. Kadhim, F.S.; Samsuri, A.; Idris, A.K. Using well logging data to predict permeability of a complex formation. *Int. J. Pet. Eng.* **2017**, *3*, 1–13. [[CrossRef](#)]
44. Mjili, A.S. Petrophysical analysis of reservoir rocks at mlinzi mbali-1 well in block 7 offshore, Tanzania. *Open J. Geol.* **2018**, *8*, 764–780. [[CrossRef](#)]
45. Mennan, A. Well Log Interpretation and 3D Reservoir Property Modeling of Maui-B Field, Taranaki Basin, New Zealand. Master's Thesis, Missouri University of Science and Technology, Rolla, MO, USA, 2017.
46. Farag, M.I.A.-F.I. Geophysical Reservoir Evaluation of Obaiyed Field, Western Desert, Egypt. Ph.D. Thesis, University of Sharjah, Sharjah, United Arab Emirates, 2010.
47. Alao, P.A.; Ata, A.I.; Nwoke, C.E. Subsurface and Petrophysical Studies of Shaly-Sand Reservoir Targets in Apete Field, Niger Delta. *Int. Sch. Res. Not.* **2013**, *2013*, 102450. [[CrossRef](#)]
48. Widarsono, B. Choice of water saturation model in log analysis and its implication to water saturation estimates—A further investigation. *Sci. Contrib. Oil Gas* **2012**, *35*. [[CrossRef](#)]
49. AlMuhaidib, A.M.; Sen, M.K.; Toksöz, M.N. Integration of geology, rock physics, logs, and prestack seismic data for reservoir porosity estimation. *Am. Assoc. Pet. Geol. Bull.* **2012**, *96*, 1235–1251. [[CrossRef](#)]
50. Burke, J.A.; Campbell, R.L., Jr.; Schmidt, A.W. The litho-porosity cross plot a method of determining rock characteristics for computation of log data. In Proceedings of the SPE Illinois Basin Regional Meeting, Evansville, Indiana, 30–31 October 1969; Society of Petroleum Engineers: Richardson, TX, USA, 1969.
51. Serra, O. *Advanced Interpretation of Wireline Logs*; Schlumberger: Houston, TX, USA, 1987.
52. Gibson, C.R. *Basic Well Log Analysis for Geologists*; American Association of Petroleum Geologists: Tulsa, OK, USA, 1982.
53. Ashraf, U.; Zhu, P.; Yasin, Q.; Anees, A.; Imraz, M.; Mangi, H.N.; Shakeel, S. Classification of reservoir facies using well log and 3D seismic attributes for prospect evaluation and field development: A case study of Sawan gas field, Pakistan. *J. Pet. Sci. Eng.* **2019**, *175*, 338–351. [[CrossRef](#)]
54. Kohonen, T.; Schroeder, M.R.; Huang, T.S. *Self-Organizing Maps*; Springer-Verlag New York Inc.: New York, NY, USA, 2001; p. 43.
55. Amanipoor, H. Providing a subsurface reservoir quality maps in oil fields by geostatistical methods. *Geod. Cartogr.* **2013**, *39*, 145–148. [[CrossRef](#)]
56. Abdideh, M.; Ameri, A. Cluster analysis of petrophysical and geological parameters for separating the electrofacies of a gas carbonate reservoir sequence. *Nat. Resour. Res.* **2019**, *29*, 1843–1856. [[CrossRef](#)]
57. Cornish, R. Statistics: Cluster analysis. *Math. Learn. Support Cent.* **2007**, *3*, 1–5.
58. Hussain, M.; Ahmed, N.; Chun, W.Y.; Khalid, P.; Mahmood, A.; Ahmad, S.R.; Rasool, U. Reservoir characterization of basal sand zone of lower Goru Formation by petrophysical studies of geophysical logs. *J. Geol. Soc. India* **2017**, *89*, 331–338. [[CrossRef](#)]
59. Chang, H.-C.; Kopaska-Merkel, D.C.; Chen, H.-C. Identification of lithofacies using Kohonen self-organizing maps. *Comput. Geosci.* **2002**, *28*, 223–229. [[CrossRef](#)]
60. El-Din, E.S.; Mesbah, M.A.; Kassab, M.A.; Mohamed, I.F.; Cheadle, B.A.; Teama, M.A. Assessment of petrophysical parameters of clastics using well logs: The Upper Miocene in El-Wastani gas field, onshore Nile Delta, Egypt. *Pet. Explor. Dev.* **2013**, *40*, 488–494. [[CrossRef](#)]
61. Hakimi, M.H.; Al Qadasi, B.A.; Al Sharrabi, Y.; Al Sorore, O.T.; Al Samet, N.G. Petrophysical properties of Cretaceous clastic rocks (Qishn Formation) in the Sharyoof oilfield, onshore Masila Basin, Yemen. *Egypt. J. Pet.* **2017**, *26*, 439–455. [[CrossRef](#)]
62. Qadri, S.M.T.; Islam, M.A.; Shalaby, M.R. Application of well log analysis to estimate the petrophysical parameters and evaluate the reservoir quality of the Lower Goru Formation, Lower Indus Basin, Pakistan. *Geomech. Geophys. Geo-Energy Geo-Resour.* **2019**, *5*, 271–288. [[CrossRef](#)]
63. Siripitayananon, P.; Chen, H.-C.; Hart, B.S. A New Technique for Lithofacies Prediction: Back-Propagation Neural Network. In Proceedings of the ACMSE: The 39th Association of Computing and Machinery South Eastern Conference, Citeseer, Atlanta, GA, USA, 16–17 March 2001; pp. 31–38.
64. Chikhi, S.; Batouche, M. Probabilistic neural method combined with radial-bias functions applied to reservoir characterization in the Algerian Triassic province. *J. Geophys. Eng.* **2004**, *1*, 134–142. [[CrossRef](#)]
65. Ali, M.; Jiang, R.; Ma, H.; Pan, H.; Abbas, K.; Ashraf, U.; Ullah, J. Machine learning-A novel approach of well logs similarity based on synchronization measures to predict shear sonic logs. *J. Pet. Sci. Eng.* **2021**, *203*, 108602. [[CrossRef](#)]
66. Stundner, M.; Oberwinkler, C. Self-Organizing Maps for Lithofacies Identification and Permeability Prediction. In Proceedings of the SPE Annual Technical Conference and Exhibition, Houston, TX, USA, 26–29 September 2004; Society of Petroleum Engineers: Richardson, TX, USA, 2004.



67. Hussain, M.; Liu, S.; Ashraf, U.; Ali, M.; Hussain, W.; Ali, N.; Anees, A. Application of Machine Learning for Lithofacies Prediction and Cluster Analysis Approach to Identify Rock Type. *Energies* **2022**, *15*, 4501. [CrossRef]
68. Hussain, W.; Pan, L.; Wang, X.; Saqlain, M.; Ali, M.; Sadaf, R. Evaluation of unconventional hydrocarbon reserves using petrophysical analysis to characterize the Yageliemu Formation in the Yakela gas condensate field, Tarim Basin, China. *Arab. J. Geosci.* **2022**, *15*, 1635. [CrossRef]
69. Ali, J.; Ashraf, U.; Anees, A.; Peng, S.; Umar, M.U.; Thanh, H.V.; Khan, U.; Abioui, M.; Mangi, H.N.; Ali, M.; et al. Hydrocarbon Potential Assessment of Carbonate-Bearing Sediments in a Meyal Oil Field, Pakistan: Insights from Logging Data Using Machine Learning and Quanti Elan Modeling. *ACS Omega* **2022**, *7*, 39375–39395. [CrossRef]
70. Asquith, G.B.; Krygowski, D.; Gibson, C.R. *Basic Well Log Analysis (Volume 16)*; The American Association of Petroleum Geologists: Tulsa, OK, USA, 2004.
71. Ravanshad, M.S.; Soleimani, B.; Larkee, E.; Soleimani, M. Petrophysical evaluation and reservoir quality of ilam formation (late cretaceous), ahvaz oil field, dezfoul embayment, SW Iran. *Pet. Coal* **2017**, *59*, 135–145.
72. Hong-bo, L.I.; Meijun, W.T.L.I. Tracing study on oil-gas filling pathways of Yakela gas condensate field in Tabei uplift. *Acta Pet. Sin.* **2013**, *34*, 219–224.
73. Abdel-Fattah, M.I. Petrophysical characteristics of the messinian abu madi formation in the baltim east and north fields, offshore Nile delta, Egypt. *J. Pet. Geol.* **2014**, *37*, 183–195. [CrossRef]
74. Anyiam, O.A.; Andrew, P.J.; Okwara, I.C. Assessment of the heterogeneity and petrophysical evaluation of reservoirs in the “Akbar Field”, Niger Delta, Nigeria. *J. Pet. Explor. Prod. Technol.* **2017**, *7*, 1035–1050. [CrossRef]
75. Mbagu, D.E.; Mwendenu, G. Effect of Shale Volume on the Porosity of Clastic Reservoirs. Case-Study from Mkuki-1 Reservoir, Offshore Tanzania. In Proceedings of the Fifth International Conference on Fault and Top Seals, Palermo, Italy, 8–12 September 2019; European Association of Geoscientists & Engineers: Utrecht, The Netherlands, 2019; Volume 2019, pp. 1–5.
76. Paul, W.J. Petrophysics. Geology Department of Geology and Petroleum Geology University of Aberdeen. 2012. Available online: [https://www.academia.edu/40407518/Contents\\_Copyright\\_Petrophysics\\_MSc\\_Course\\_Notes](https://www.academia.edu/40407518/Contents_Copyright_Petrophysics_MSc_Course_Notes) (accessed on 24 January 2023).
77. Pirson, S.J. *Geologic Well Log Analysis*, 3rd ed.; Gulf Pub. Co.: Houston, TX, USA, 1983; p. 424.
78. Moradi, S.; Moeini, M.; Al-Askari, M.K.G.; Mahvelati, E.H. Determination of Shale Volume and Distribution Patterns and Effective Porosity from Well Log Data Based On Cross-Plot Approach for A Shaly Carbonate Gas Reservoir. In Proceedings of the IOP Conference Series: Earth and Environmental Science, Bandung, Indonesia, 28 March–2 April 2016; IOP Publishing: Bristol, UK, 2016; Volume 44, p. 42002.
79. Hamada, G.M. An integrated approach to determine shale volume and hydrocarbon potential in shaly sand. In Proceedings of the SCA International Symposium, 1996; pp. 2093–2107. Available online: <http://www.jgmaas.com/SCA/1996/SCA1996-41.pdf> (accessed on 24 January 2023).
80. Clavaud, J.-B.; Nelson, R.; Guru, U.K. Field Example of Enhanced Hydrocarbon Estimation in Thinly Laminated Formation with a Triaxial Array Induction Tool: A Laminated Sand-Shale Analysis with Anisotropic Shale. In Proceedings of the SPWLA 46th Annual Logging Symposium, New Orleans, LA, USA, 26–29 June 2005; Society of Petrophysicists and Well-Log Analysts: Houston, TX, USA, 2005.
81. Sams, M.S.; Andrea, M. The effect of clay distribution on the elastic properties of sandstones. *Geophys. Prospect.* **2001**, *49*, 128–150. [CrossRef]
82. Thomas, E.C.; Stieber, S.J. The distribution of shale in sandstones and its effect upon porosity. In Proceedings of the SPWLA 16th Annual Logging Symposium, New Orleans, LA, USA, 4–7 June 1975; Society of Petrophysicists and Well-Log Analysts: Houston, TX, USA, 1975.
83. Kurniawan, F. Shaly Sand Interpretation Using CEC-Dependent Petrophysical Parameters. Ph.D. Thesis, Louisiana State University, Baton Rouge, LA, USA, 2005.
84. Al-Jawad, S.N.; Saleh, A.H. Flow units and rock type for reservoir characterization in carbonate reservoir: Case study, south of Iraq. *J. Pet. Explor. Prod. Technol.* **2020**, *10*, 1–20. [CrossRef]
85. Gunter, G.W.; Finneran, J.M.; Hartmann, D.J.; Miller, J.D. Early determination of reservoir flow units using an integrated petrophysical method. In Proceedings of the SPE Annual Technical Conference and Exhibition, San Antonio, TX, USA, 5–8 October 1997; Society of Petroleum Engineers: Richardson, TX, USA, 1997.
86. Salman, S.M.; Bellah, S. Rock typing: An integrated reservoir characterization tool to construct a robust geological model in Abu Dhabi carbonate oil field. In Proceedings of the SPE/EAGE Reservoir Characterization & Simulation Conference, Abu Dhabi, United Arab Emirates, 19–21 October 2009; European Association of Geoscientists & Engineers: Utrecht, The Netherlands, 2009; p. cp-170.
87. Nabawy, B.S.; Barakat, M.K. Formation evaluation using conventional and special core analyses: Belayim Formation as a case study, Gulf of Suez, Egypt. *Arab. J. Geosci.* **2017**, *10*, 25. [CrossRef]
88. Manzoor, U.; Ehsan, M.; Radwan, A.E.; Hussain, M.; Iftikhar, M.K.; Arshad, F. Seismic driven reservoir classification using advanced machine learning algorithms: A case study from the lower Ranikot/Khadro sandstone gas reservoir, Kirthar fold belt, lower Indus Basin, Pakistan. *Geoenery Sci. Eng.* **2023**, 211451. [CrossRef]



89. Tounkara, F.; Ehsan, M.; Nasar Iqbal, M.; Al-Ansari, N.; Hajana, M.I.; Shafi, A.; Elbeltagi, A. Analyzing the seismic attributes, structural and petrophysical analyses of the Lower Goru Formation: A case study from Middle Indus Basin Pakistan. *Front. Earth Sci.* **2023**, *10*. [[CrossRef](#)]
90. Munir, M.N.; Zafar, M.; Ehsan, M. Comparative and Statistical Analysis of Core-Calibrated Porosity with Log-Derived Porosity for Reservoir Parameters Estimation of the Zamzama GAS Field, Southern Indus Basin, Pakistan. *Arab. J. Sci. Eng.* **2022**. [[CrossRef](#)]

**Disclaimer/Publisher's Note:** The statements, opinions and data contained in all publications are solely those of the individual author(s) and contributor(s) and not of MDPI and/or the editor(s). MDPI and/or the editor(s) disclaim responsibility for any injury to people or property resulting from any ideas, methods, instructions or products referred to in the content.